Archives of Materials Science and Engineering

Volume 53
Issue 1
January 2012
Pages 5-28

International Scientific Journal
published monthly by the
World Academy of Materials
and Manufacturing Engineering

Polymer nanocomposites reinforced with montmorillonite

L.A. Dobrzański [a,*], M. Bilewicz [a], J.C. Viana [b]

[a] Institute of Engineering Materials and Biomaterials, Silesian University of Technology, ul. Konarskiego 18a, 44-100 Gliwice, Poland

[b] Institute for Polymers and Composites, Department of Polymer Engineering, University of Minho, 4800-058 Guimaraes, Portugal

* Corresponding e-mail address: leszek.dobrzanski@polsl.pl

Received 11.10.2011; published in revised form 01.01.2012

ABSTRACT

Purpose: Light microscope with polarized light has been used for observation layered zone, visible thanks to polarization of the light, inside polymer-polymer composites and nanocomposites Aim of work has been concentrated on investigation of nanocomposites as promising engineering materials, basing on composition of polypropylene and montmorillonite as reinforcement in the shape of nanoparticles of 2:1 silicate.

Design/methodology/approach: Conventional and non-conventional injection molding process has been used for obtaining nanocomposites. In non-conventional process has been used the special mold for inducing the shear rates, additionally equipped with external computer to control melt manipulation of solidifying polymer inside mold cavity

Findings: Highly developed structure consisted of multilayer zone between skin and core mainly responsible for reinforcement and improvement of fracture toughness of polymer composites and nanocomposites

Research limitations/implications: Nanocomposites of polymer blends and montmorillonite were moulded by direct injection moulding according to melt temperature and stroke time-number combination included in design of experiments.

Practical implications: Application of special injection moulding technique provides to structure development and gives possibility to create multilayer zone, which strengthen material. Besides strengthening obtaining of such nanocomposites is cheap thanks to application of low cost injection moulding technique and not expensive polyolefines with developed structure, without using additional fillers (e.g. compatybilizers).

Originality/value: Very wide application of polymer composites and nanocomposites as engineering materials used for various industries like building engineering, automotive and aerospace

Keywords: Polymer-polymer composites; Polymer processing; Engineering polymers; Injection moulding

Reference to this paper should be given in the following way:

L.A. Dobrzański, M. Bilewicz, J.C. Viana , Polymer nanocomposites reinforced with montmorillonite, Archives of Materials Science and Engineering 53/1 (2012) 5-28.

RESEARCH MONOGRAPH

1. Introduction

Demand for sophisticated engineering materials in wide range of applications, like automotive, aerospace and building sector creates a need for looking for new and developing existing materials, basing on cost analysis, engineering development and performance requirements [1-9]. In many R & D centres researchers try to develop existing or create new structures through design of new alloys or composites, application of neural networks and artificial intelligence tools, looking simultaneously for better, improved properties of materials [10-18. 71]. Relation of the strength of material to its weight is one of the key aspects of materials selection, whereby may be construct tough components, concurrently with less and less weight. Comparison of the relative strength of selected engineering materials shows that metal alloys and polymer composites are reinforced with diversified particles and fibres, and highly developed (Fig. 1) [19-26].

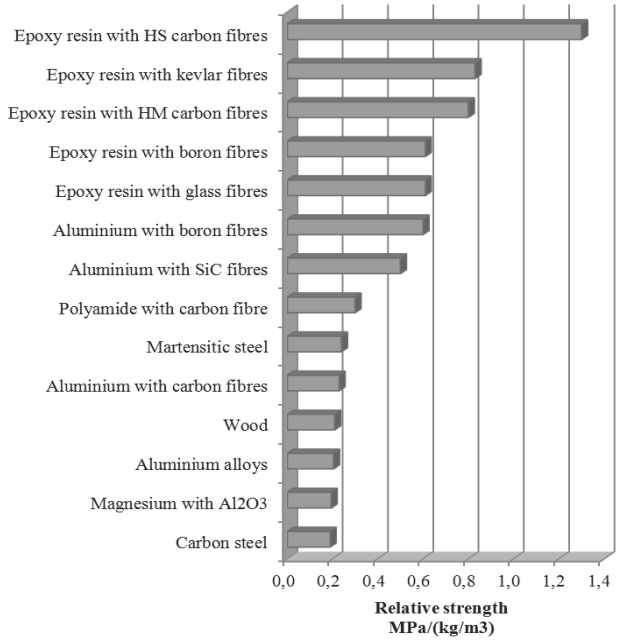

Fig. 1. Comparison of relative strength of selected engineering materials, including composites [69]

In connection with these necessities nowadays common potential group of materials are metals, light alloys and polymer composites and nanocomposites [27-34, 72-75, 78]. The last ones have possibilities of simple shape giving, material's selection for matrix and reinforcement and thanks to low cost of materials, their application is also beneficial from economical point of view [35-43].

According to report of branch experts and futurologists for present and future plastic market evolution growth of consumption of plastics will keep upward trend until 2020, reaching demand level equal to 300 million tons, which shows a 16% increase comparing to 2010 (demand equal to 250 million tons) (Fig. 2) [44].

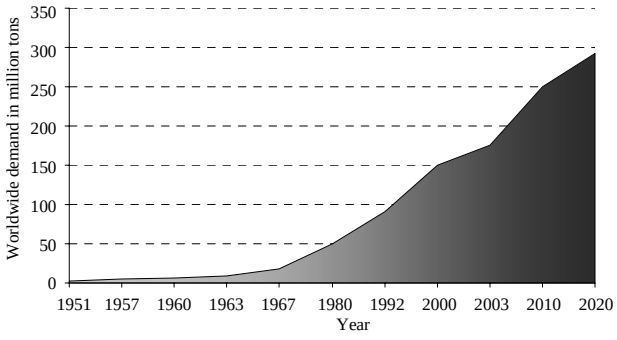

Fig. 2. Worldwide demand for polymeric materials [44]

Consumption of polymeric materials is increasing as well and reaches up to 120 kg per person (Fig. 3).

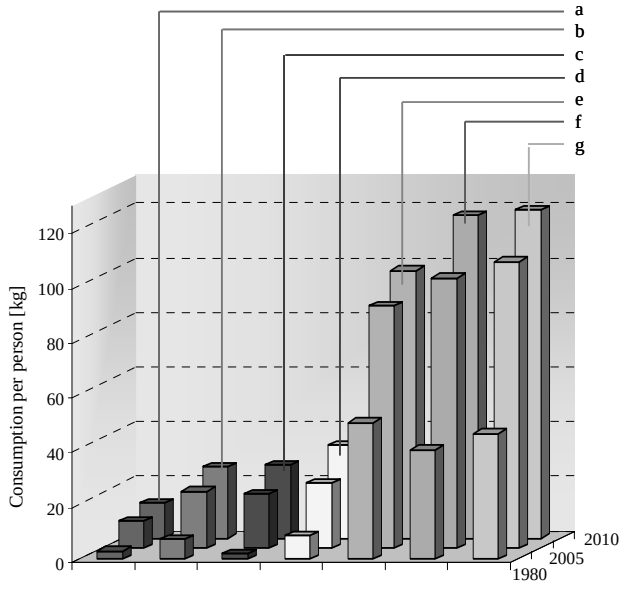

Fig. 3. Consumption of polymers per person for different regions; a – Middle East and Africa, b – Latin America, c – Asia without Japan, d - Central and Eastern Europe, e – Japan, f – Western Europe, g – NAFTA (North American Free Trade Agreement) [45]

One of the most common and economical technique of processing polymers is undoubtedly injection moulding process which grows on many sectors including medical, shipbuilding, aerospace and automotive components, consumer products for daily use, construction and packaging, becoming the major part of the plastic industry worldwide. Global expenditure of all plastics is approximately 32 wt%, what can be observed in the world's annual consumption of these materials, which has increased from around 5 million tons in the 1950s to nearly 100 million tons nowadays. Injection moulding is then process that allows production of cheap and day by day more durable components, and manufacturers occupy a significant place in directing the trends and global development of manufacturing and processing of polymeric materials [3, 45, 46].

There is also continuous growth of units of injection moulding machines on worldwide market with total 95 000 of units of injection moulding machines in 2010, with the value of about 7000 million euro, up to 140 000 in 2013, with the value of more than 9000 million euro, thanks to the demand of moulders in Eastern, Southern and Northern Europe, China, Latin America and India [47, 48].

Mostly production of polymers is concentrated on packaging, both in Poland and in Europe in 2009 and 2010 respectively, ranging up to 40%, and nextly on building, other products (sport, recreation, agriculture, manufacture of machinery), automotive and electric and electronic devices (Figs. 4, 5).

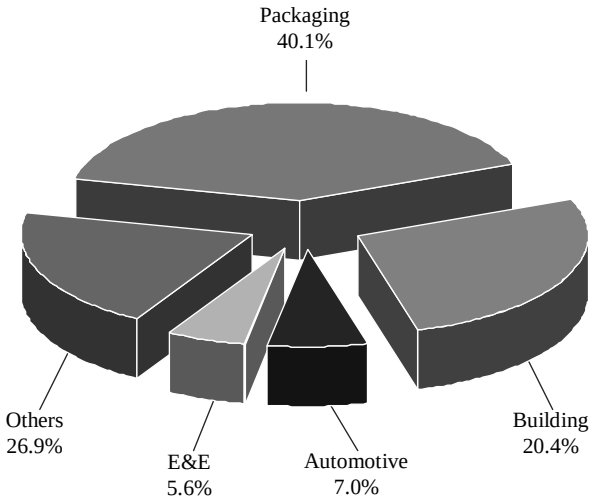

Fig. 4. Plastics application in Europe [46, 49]

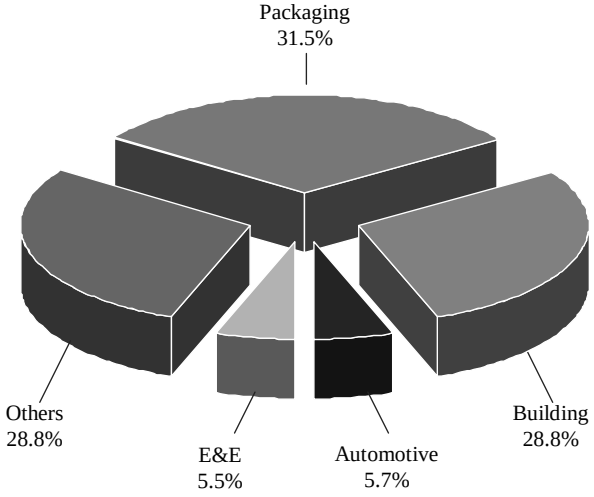

Fig. 5. Plastics application in Poland [47, 50]

The mechanical and physical properties of polymer composites and nanocomposites arise not just from the combination of polymer compounds, but also from the morphologies development (e.g., at the interface of the matrix).

Furthermore, eventual polymer-polymer reactions (e.g., copolymer formation, considering also immiscible polymer blends in which are included most of the polymer combinations) occurring due to the thermomechanical treatment applied during processing (e.g., injection moulding) expand range of tailoring of structure through mechanical performance.

The diversity of morphology can be additionally specified by the shape (rod, sphere or plate), size (micro, nano) and distribution of dispersed particles in the matrix. This fact made a contribution in development of polymer processing worldwide. Polymers and composites/nanocomposites based on polymer matrix can be produced and processed by many techniques. The mostly known polymer processes includes:

- Extrusion,
- Injection moulding,
- Injection blow moulding,
- Reaction Injection Moulding (RIM),
- Rotational moulding,
- Co-injection Moulding,
- Expansion bead moulding,
- Extrusion blow moulding,
- Gas Assisted Injection Moulding (GAIN),
- Compression moulding,
- Powder Injection Moulding,
- Liquid resin moulding techniques (LRM),
- Resin transfer moulding (RTM),
- Vacuum injection moulding (VIM),
- Thermal-expansion resin transfer moulding (TERTM),
- Spray-up moulding,
- Hand lay-up,
- Sheet thermoforming,
- Vacuum forming,
- Pressure forming,
- Steam pressure forming.

During the processing stages of the injection moulding cycle the polymer is subjected to a severe thermomechanical environment, comprising high cooling rates and stress levels, determined by:

- material properties (e.g., thermal, rheological),
- geometry of the moulded piece (e.g., thickness, flow length),
- the mould design options (e.g., feeding system geometry, size and location of the gate),
- the moulding equipment operation (e.g., set-up conditions, constructive aspects) [51-53, 76-77].

Specific configuration of all mentioned above variables and parameters upon cooling stage extorts development of the material's structure, and during this process is involved complex relaxation and crystallization phenomena, both highly dependent on the imposed thermal and stress fields. Consequently an injection moulding features a complex structural gradient with a spatial variation within the entire confined domain, especially in the case of semicrystalline polymers. Moreover to the polymers can be also added stabilizers, lubricants, flame retardants, fillers, coupling or antistatic agents, pigments and different reinforcing elements for changing and improving optical, mechanical or chemical properties, such change of colour and glance, improvement of processing, conductivity, strength, stiffness, bonding between matrix and filler or preclude deterioration by ultra-violet light [54-60].

Polymer composites and nanocomposites are designed mainly by selection of the type of polymeric components, which constitute the overwhelming majority of the composite mass and by the selection of technology production. However, other materials may be added including compatibilizers, for better compatibility of immiscible polymers (e.g. PP with PS) and particles with micro- and nano size, working as reinforcement of composite. Reactions occurring due to the injection moulding process, where high shear rates appear, may enable structural changes without addition of particles or compatibilizating agents. Structures of injected polymers obtained under different processing set-up depends on characteristic parameters like heating-cooling rates, injection velocity, pressures (back pressure, holding pressure) and geometric dependences (screw diameter, capacity of the mould). Static crystallization creates spherulitic structure and has effect on processing temperatures. Applying additional deformation of material (e.g. when stress appears) change the behaviour of material and finally also influences the structure. High shear stress during solidifying stage brings developed morphology, like multilaminar structure or reinforced polymer-polymer composites. Through controlling the process can be achieved control of the structure and hence control of mechanical properties. Injection moulding as quick process to manufacture high quality of large number of parts is one of most common techniques used in processing of polymers worldwidely, however there are important limitations of conventional injection moulding, including the constricted range of controlled stress level imposed to the melt during the filling and holding stage of the injection process, therefore non-conventional injection moulding techniques are in wide demand [61-65].

Application of products obtained by conventional and non-conventional injection moulding, also with use of rotational or multicavity moulds, starts at domestic level of products and finishes with advanced engineering materials and composites, used in automotive, aerospace and building sectors. Solidifying polymer subjected to flow inside mould cavity, during its crystallizing and solidifying phase and undergo to high shear rates, creates developed structure with skin-core zones, more oriented than structure obtained by conventional injection moulding process. Creation of morphology depends then on moulding processing setup and polymer properties as well. Molten polymer is subjected to shear and elongational flow, prior to crystallization. Closer to frozen layer at mould side shear rate dramatically increases and formation of extended particles is reported accordingly to the profile of shear rate and melt flow model. The challenging area is reinforcing polymer composites by compounding nanofillers with polymer matrix e.g. iPP by melt mixing through extruding and further forming or injection moulding by direct forming desired shape. There are many possibilities of forming nanocomposites, but the main goal for all techniques is good exfoliation of particles and in effect improvement of mechanical properties. Fragmentation of agglomerated particles and well distribution can be obtained by inducing high shear into processing. This element of production is satisfied by non-conventional injection moulding process, used in this experiment, where in the shear zone and especially on the layers' boundaries exist high shear rates, additionally intensified by transportation of melt flow front along quasi-frozen layer [66-68].

For easier identification of abbreviations, occurring in the article, explanations will be included in the Table 1.

Table 1.
List of abbreviations used in article

	Material
iPP	Isotactic polypropylene
MMT	Montmorillonite (distearyl-dimethyl-ammonium ion exchanged bentonite)
	Processing
CIM	Conventional Injection Moulding
N-CIM	Non-conventional IM
	Experiment
St	Stroke time
Sn	Stroke number
Tm	Melt temperature
PLM	Polarized Light Microscopy

2. Materials and methods

In the experiment polypropylene (iPP) as matrix material has been used and as reinforcing filler was added montmorillonite (MMT) to the particular compositions. In the experiment was chosen two research direction – change of processing and change of material composition. For this reason polypropylene was mixed with nanoparticles at different ratio. Comparison of results was basing then on comparison of five different nanocomposites with variable ratios of materials and neat PP as base material for comparison the results (Table 2, Fig. 6). Specifications of materials are listed below (Table 3).

Table 2.
List of investigated composites arranged by wt% of particular material

Nr	Abbreviation	PP	MMT
1	Neat PP	100	-
2	PP/MMT 0.5	99.5	0.5
3	PP/MMT 1	99	1
4	PP/MMT 3	97	3
5	PP/MMT 5	95	5
6	PP/MMT 10	90	10

Table 3.
Materials used in experiment

Material	Grade	Suppliers	Characteristics
PP	Moplen HP501M	Bassell	density: 0.9 g/cm^3 melt temperature: 200ºC
MMT	Nanofil 5	Süd-Chemie	density: 1.8 g/cm^3 melt temperature: >390ºC particle size: ≈1×300×300 nm

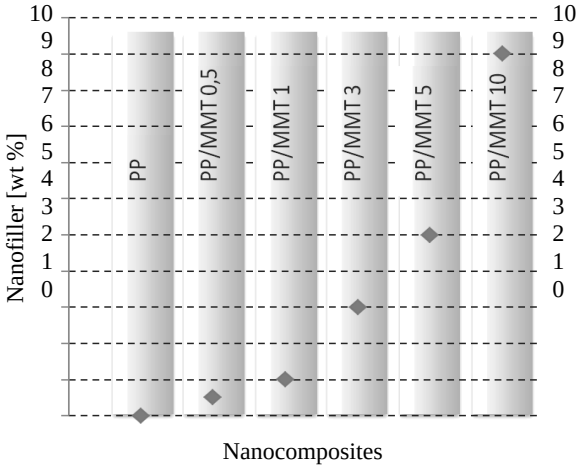

Fig. 6. Increment of nanofiller quantity in polymer matrix

In the experiment has been used montmorillonite - nanosized clay with a layered structure divided on two tetrahedral sheets bonded to octahedral between them sheets, containing atoms of aluminium, silica and magnesium, described by formula: $M_x(Al_{4-x}Mg_x)Si_8O_{20}(OH)_4AlO_6$. Montmorillonite as common smectite clay contains arrangement of these sheets in proportion 2:1 (Fig. 7).

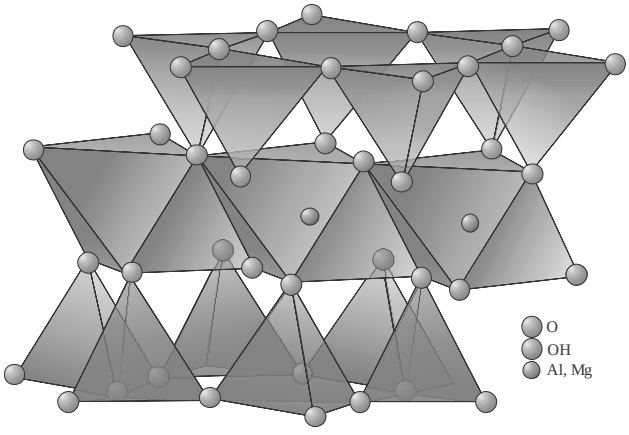

Fig. 7. Schematic illustration of atoms arrangements in a typical MMT layer

These nanofillers are incorporated into the matrix or in the composite to improve or modify optical, mechanical or physical properties. Nanocomposites reinforced by montmorillonite can be obtained by direct polymer melt intercalation or exfoliation. During this process polymer chains diffuse into the space between the clay galleries, and fully separated the clay nanolayers, respectively. Normally the apparent crystallinity increases with filler content and becomes asymptotic for more than 2-5% of the filler concentration [4].

Blending of PP/MMT was conducted by mixing dried materials in the barrel at rotor speed equal to 60 rpm and in the room temperature and then located in the feeder of moulding machine. After compounding, blends were injection moulded into standard rectangular bar prepared for bending test.

Experimental plan has been set accordingly to design of experiment, to determines interactions between factors (like settings of machine or types of material) affecting injection moulding process and output of that process, e.g. mechanical properties. Basing on these outputs can be easily indicated settings to obtain best properties and also predict future changes for better optimization of the process. Settings were adjusted for two injection moulding techniques conventional and non-conventional basing on minimum and maximum values of changeable parameters (Fig. 8).

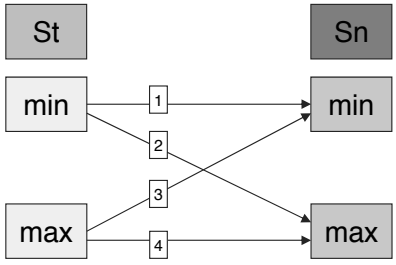

Fig. 8. Design of experiment basing on two levels - minima and maxims of changeable parameters of non-conventional injection moulding process – stroke time and stroke number at constant temperature

Combination between three changeable processing parameters, that is – melt temperature, stroke time and stroke number, gives eight sets for non-conventional technique and two sets for conventional one (Table 4). Therefore has been obtained 10 sets of processing variables, what gives total amount of 60 different nanocomposites with diversified amount of nanoparticles and processed under different conditions.

Accordingly to the experimental plan has been chosen 2 levels for each parameter, that is 240°C and 280°C for melt temperature, 1 and 3 second for stroke time and for stroke number 3 and 12 strokes (Table 5).

Table 4.
Sets of parameters for non-conventional and conventional injection moulding technique

	Set	Tm, °C	St, s	Sn
N-CIM	1	min	min	min
	2	min	max	min
	3	min	min	max
	4	min	max	max
	5	max	min	min
	6	max	max	min
	7	max	min	max
	8	max	max	max
CIM	1	min	-	-
	2	max	-	-

Table 5.
Set of parameters for N-CIM and CIM

Technology	Set	Settings of the processing parameters		
		Tm, °C	St, s	Sn
N-CIM	1	240	1	3
	2	240	3	3
	3	240	1	12
	4	240	3	12
	5	280	1	3
	6	280	3	3
	7	280	1	12
	8	280	3	12
CIM	1	240	-	-
	2	280	-	-

One second for stroke time has been set as the minimum value and the higher value has been set for 3 seconds, to keep relatively short time of the whole process. Similarly as for dependence between low and high values of St, 3 and 12 strokes has been set for Sn. Shear time which influences on the structure is the multiplication of St and Sn. Creation of one skin layer in the structure at one side of the obtained mould is typical for CIM process, where highest level of shear stress exists in to the outer side close to the skin (Fig. 9). This phenomenon, mentioned in literature by D. Rosato and L.A. Utracki [3, 70], considers fact, that particles located closer to skin are extended due to faster cooling and simultaneously strong shearing.

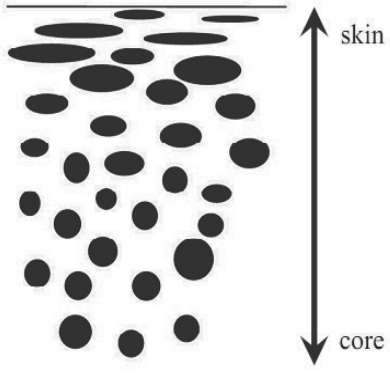

Fig. 9. Cross section of the moulding and shape of particles across the specimen, influenced by shear during injection [71]

Preliminary research approved this phenomena and was the basis for further research and continuation of the undertaken issue (Fig. 10).

The same effect can be achieved during N-CIM process and multiplied, until melt is not solidified, due to repeating sequences of reciprocating movements developing the structure through creating the shear zone and inducing shape modification of particles. To get developed structure and basing on this phenomena, at least three strokes as minimum Sn parameter in N-CIM process, have to be set, to obtain more than one layer, basing simultaneously on high shear rate treatment of the melt in outer region. Maximum of the strokes' number shouldn't extend total processing time, taking into consideration, that each stroke takes 1 second. After preliminary tests, 12 strokes have been chosen as upper limit, and gave possibility to obtain up to 11 layers (Fig. 11).

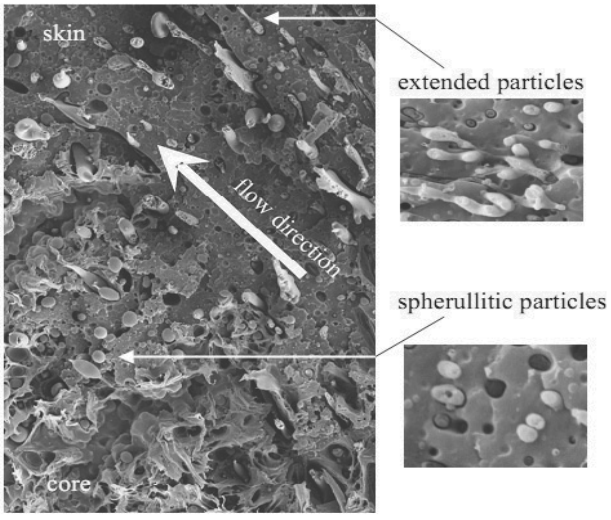

Fig. 10. Cross section of the moulding with visible spherulitic and extended shape of particles across the specimen, subjected to different shear rates

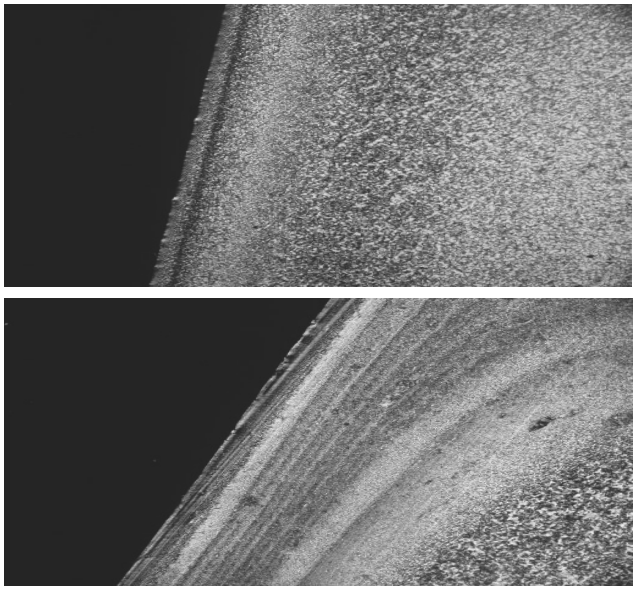

Fig. 11. Cross section of the moulding performed by CIM and N-CIM technology with visible typical skin-core structure for CIM (top figure) and highly extended multilayer structure obtained by N-CIM (bottom figure)

Injection moulding process for all specimens has been done by using conventional and non-conventional process, where the second one has been used to induce multilayer structure. Blends' composition was used subsequently in the non-conventional injection moulding technique performed on specially adopted injection machine. N-CIM process consists on the handling of the melt polymer, which is provided through two hot-runner channels, and induces high shear rates by using various movements of external pistons to obtain outer, highly oriented multilayer zone and a less oriented inner core in the structure of the moulding (Table 6).

Table 6.
Set of variable and constant parameters for N-CIM process

N-CIM			
	Varied parameters		
		min	*max*
Mode A *(reciprocation)*	Stroke time, s	1	3
	Stroke number	3	12
Mode B *(holding)*	Constant parameter		
	Cooling time, s	30	

For experiment has been used injection pressure of 150 bar. Each set-up is finished by this mode. There is also possibility to use mode for compressing and extracting, which wasn't use in this experiment. All other parameters included in the moulding programme, namely velocity of injection, hydraulic pressure, cooling time (equal to stage time of mode C) were kept constant (Table. 7).

Table 7.
Constant injection processing set-up (machine readings)

Injection velocity	10 mm/s
Injection pressure	150 bar
Holding pressure	50 bar
Mold temperature	30°C
Cooling time	30 s

The temperature profile of heating units of machine, detected by barrels sensors and controlled via computer, has been prepared for two levels (Fig. 12, Table 8). Temperature of the mould, as part of N-CIM process, controlled by independent managing system, was detected by sensors mounted in the walls of the mould.

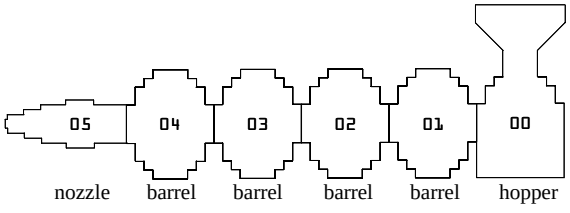

Fig. 12. Heating zones of injection moulding machine

To the main stages, which make up the injection moulding process, can be included:

- implementation of the material, in a granulate or powder form, to the feeder,
- transfer of the material by screw through the heated barrels,
- plasticizing of the material,
- clamping of the mould,
- injection of the melted material into mould's cavity,
- solidification of material during cooling stage inside cavity,
- plasticizing during withdrawal of the screw of the next portion of material to be ready for next injection,
- ejection of the moulding.

Table 8.
Temperature profile of processing for two levels

Machine unit	Mould	Nozzle	Barrel 4	Barrel 3	Barrel 2	Barrel 1	Hopper
Min, °C	30	240	230	220	210	200	40
Max, °C	30	280	270	260	250	240	40

To modify and develop this process, typical mould has been replaced by special one, externally operated by the computer and pressure machine (generating 150 bar hydraulic pressure) (Fig. 13). The pressure machine, with computer aided system, controls reciprocation of the piston movements, actuated by pressure transmitted trough pressure hoses to the mould. The whole system controls flow of melt polymer during solidification. Shear rate induced during this stage influences morphology and causes creation of multilayer zone. The number of layers is dictated by set of piston movements, namely by two parameters – number and time between feeds.

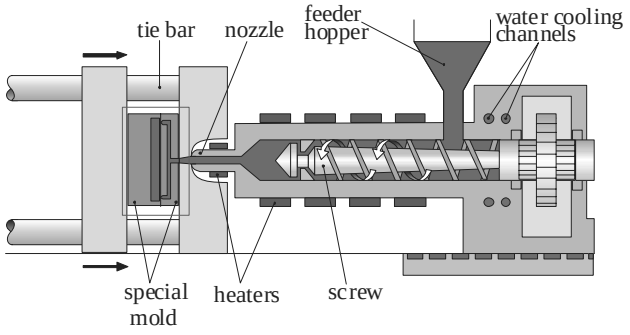

Fig. 13. Injection moulding machine with indication on replaced mould as a key-unit in N-CIM

Typical injection moulding process consisted on injection, cooling and ejection was the first part of processing. After clamping of moveable part of mould and injection of polymer melt into cavity, cooling stage starts (Fig. 14). At the same moment N-CIM stage also begins.

The melt polymer injected into mould cavity through bifurcate runners is subjected to moving alternately by pistons (top and bottom) under high pressure. Pistons' movements were set in two modes, primary and finalizing one. The first mode consisted on alternating extension and retraction of the melt in the mould cavity (Fig. 15).

During this mode was created structure in the rectangular shape bar, composed of two phases – skin, shear zone and core,

forming highly developed morphology. The second mode was keeping permanent pressure on constant level (Fig. 16). Each process finished by this mode.

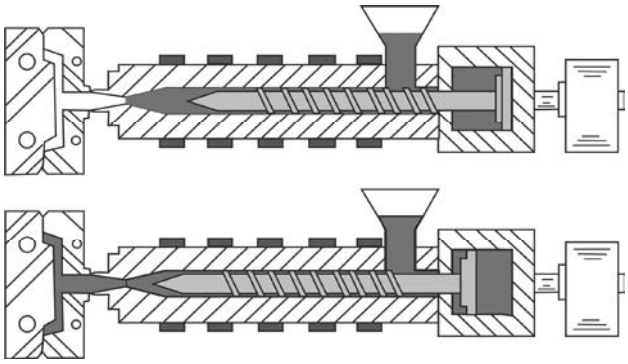

Fig. 14. First part of processing in the experiment – conventional injection moulding; implementation and plasticizing of the polymer (top figure) and injection to the mould (bottom figure)

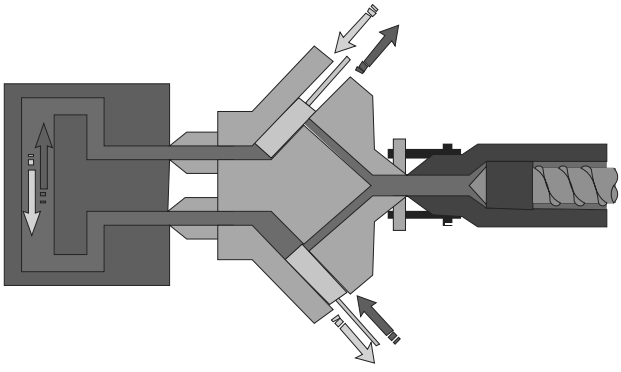

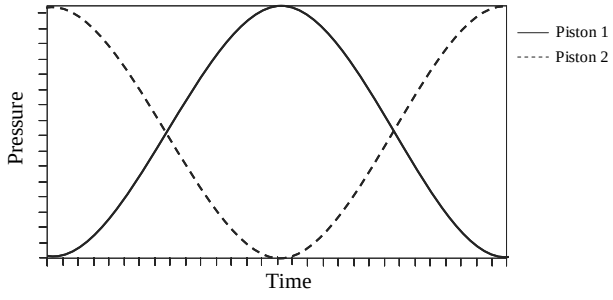

Fig. 15. The first mode of N-CIM process − alternating movement extension and retraction

Performed rectangular specimens were tested by 3-point bending test with crosshead speed 10 mm/min (according to the ASTM E399 standard) and for flexural test with crosshead speed 2.8 mm/min (ISO 178 -75) (Fig. 17). The fracture test was performed in a Instron 4505 universal testing machine at the crosshead velocity of 10 mm/min, accordingly to ASTM E399 norm. A notch 6.35 mm deep was made at a Ceast 6816 cutting machine with triangular blade with a 0.47 mm tip radius. For each processing run were tested at least five specimens to exclude extreme values in aim to possess at least three results for mean value. Aim of mechanical characterization was comparison of synergetic effects of polymer-polymer composites and influence of processing conditions on the flexural behaviour. The energy, absorbed during test, was used as comparable value between processing parameters. Air humidity (50%) and air temperature (23ºC) were kept under sTable conditions by sensor control system.

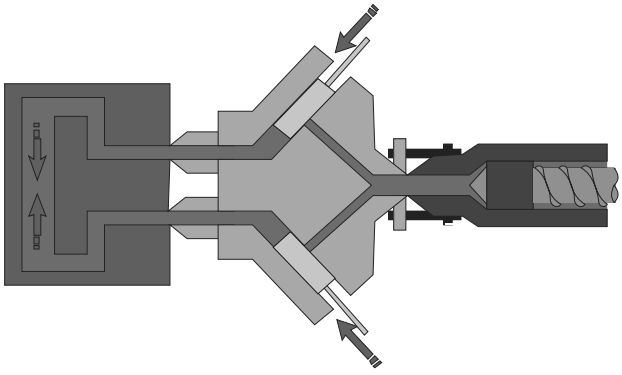

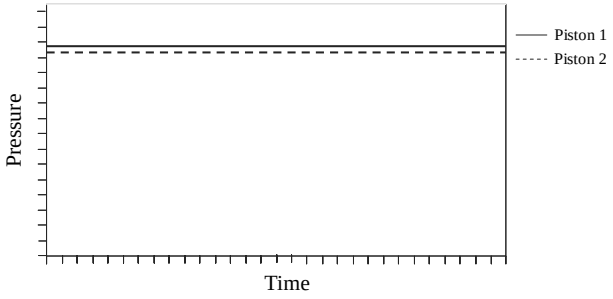

Fig. 16. The second mode of N-CIM process

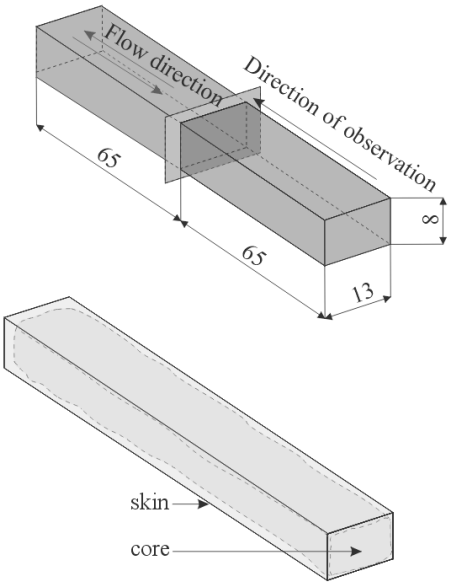

Fig. 17. Draw of the specimen with specified cross section region

Morphology of blends has been observed microscopically in polarized light, where light from a source passes polarizer and changes on plane polarized light and then crosses birefringent specimen, where light rays are split (Fig. 18). Nextly two rays - ordinary and extraordinary one, cross analyzing lens and are recombined alongside the same optical path. This technique of observation distinguishes isotropy and anisotropy of materials and, basing on these differences, delivers details about structure. In the experiment PLM was suiTable technique to detect layers.

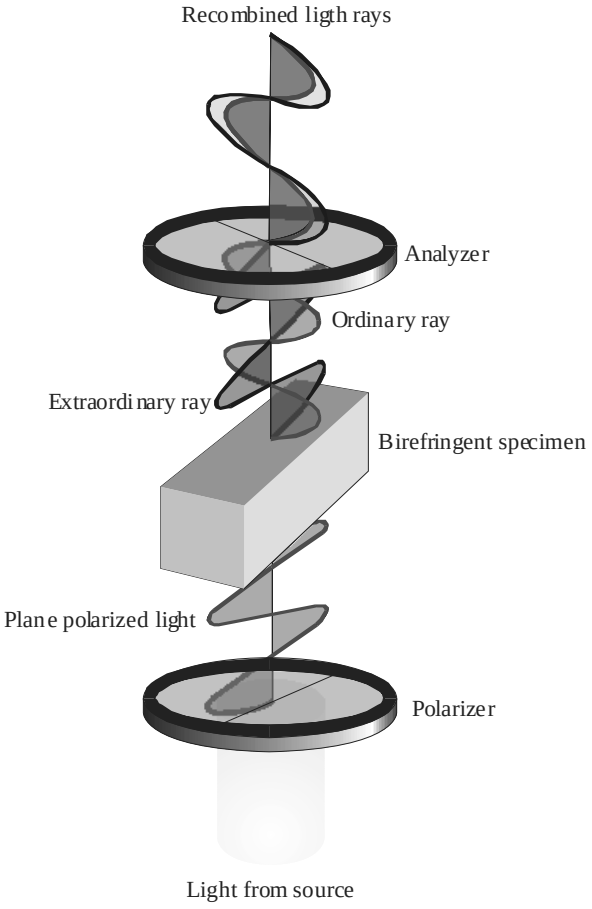

Fig. 18. Scheme of observation by using polarized light microscopy

Cross sections were chosen from the middle regions of specimens. Slices of 20 μm thick have been performed on the cut machine Microtom Anglia Scientific until suiTable quality of a surface for microscopic observation was achieved. Specimens have been observed by polarized light microscopy, electron scanning microscopy and transmission electron microscopy in the aim to understand the structure development.

Wide angle X-ray scattering (WAXS) concentrated on scattering angles 2θ larger than 10° was performed to assess the degree of crystallization of the polymer matrix and the interplanar spacing of montmorillonite galleries (Fig. 19).

The study was performed using synchrotron radiation at the line A2 for measuring soft matter in Hasylab (Hamburg) at a wavelength λ = 0154 nm (8 keV) and scan speed 0.03°/s. Measurements were made in the range of 2Θ angle: 10º-25º. The result of measurement in this method is the scattering 2Θ angle, contained between ray beam and the beam reflected from the two sequent crystallographic planes, in this case the montmorillonite platelets.

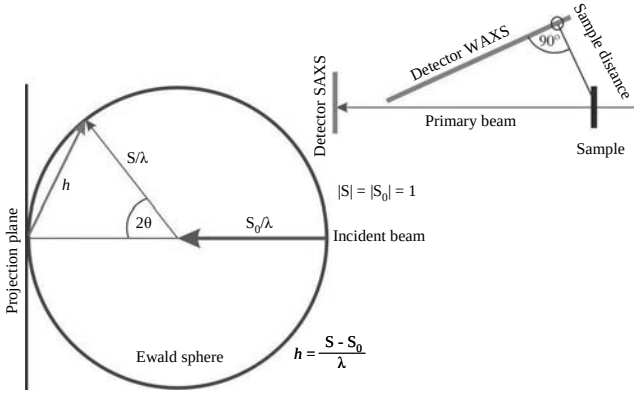

Fig. 19. Scheme of the X-ray scattering (SAXS and WAXS); Ewald sphere with a radius 1/λ, is formed by the ends of the wave vectors of bent beams, taking into account that the beginnings of vectors starting at the point of incidence of radiation on the crystal. Diffraction occurs when the reciprocal lattice, which is beginning at the point of puncture the sphere by the end of the vector of the incident beam, will be on the field

3. Discussion of experimental results

The effect of shear actions on the structural and morphological development of reinforced and non-reinforced polypropylene homopolymer was observed. For the typical case of an injection moulded centre gated disk, it is well known that the shear and extensional stress fields will vary along the flow length, leading to a variation of the molecular and fibre orientation distributions. The result is the development of a complex microstructure and reinforcement morphology within the moulding, which affects the thermo, the mechanical and other properties.

Polarized light micrographs of the specimens of the polymer nanocomposites obtained by CIM process feature a well-defined skin-core structure (Fig. 20). Image analysis allowed extracting region of the core and calculating contribution of the shear zone/skin in the specimen. Core/sheared zone ratio has been counted by using detection techniques and additionally enhanced to obtain clear image by using such kind of methods like balancing of local colours or photo-lofting (Figs. 20, 21).

Specimens performed by CIM contain big core, which occupies 90% of specimen and outer morphology consists on one external layer. That structure is typical for CIM processes. Core is then 10 times bigger than shear zone, in this case just skin (Fig. 20).

In the specimens performed by N-CIM, core occupies 52%, the rest belongs to shear zone, including skin. Visible difference between CIM and N-CIM morphology is also the shrinkage appearing in specimens processed by CIM; reciprocation of

pistons' movements in N-CIM process fulfils tightly capacity of the mould, not allowing material to shrink (Fig. 21).

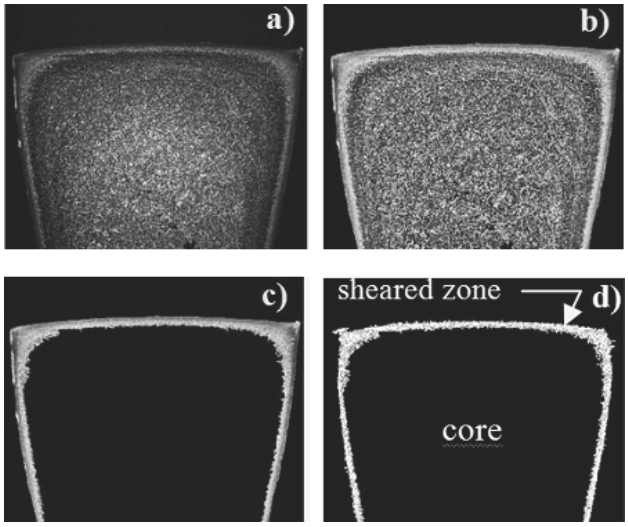

Fig. 20. Order of computer aided PLM image analysis and area calculations of cross section of specimen obtained by CIM; a) direct image from PLM, b) contrast-brightness improvement, c) edge detection, d) mask overlapping

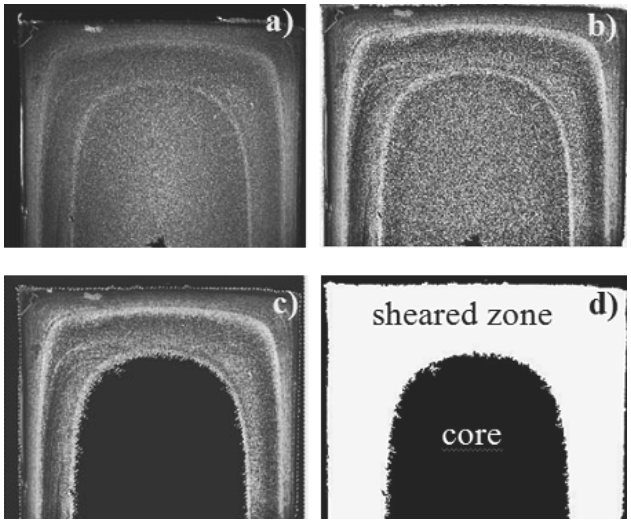

Fig. 21. Order of computer aided PLM image analysis and area calculations of cross section of specimen obtained by N-CIM; a) direct image from PLM, b) contrast-brightness improvement, c) edge detection, d) mask overlapping

Cross section of PP specimens, performed by CIM, both the low (240°C) and high (280°C) temperature, is characterized by large, spherullitic core, skin with thickness of about 300 microns and solidification shrinkage of 2% (Figs. 22, 23).

For specimens performed by N-CIM there has been reported more accurately mapping of the cavity shape and shrinkage of 0.2-0.3% (Fig. 24).

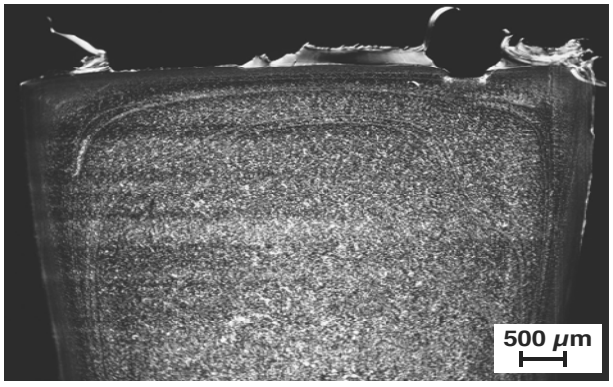

Fig. 22. Cross section of the neat PP specimen performed by CIM in 240°C

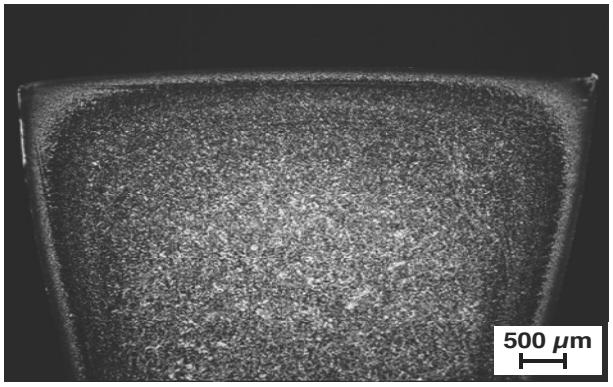

Fig. 23. Cross section of the neat PP specimen performed by CIM in 280°C

There was also no growth of shared zone, comparable with a layer of skin, covering 11% of the sample volume, for polypropylene specimens performed by N-CIM technology at low settings of changeable parameters - the melt temperature, stroke number and stroke time (set 1 and 2, accordingly to Table 9) (Figs. 24 a, b). Increment of the stroke number (set 3 and 4) (Figs. 24 c, d) and simultaneously melt temperature together with stroke number (set 5-8) (Fig. 24 e-h), created and significantly developed multi-layer sheared zone and increased to 45% of the sample volume.

Table 9.
Description of set of parameters for N-CIM and assigned abbreviations

Abbreviation	Set	Settings of the processing parameters		
		Tm, °C	St, s	Sn
a	1	240	1	3
b	2	240	3	3
c	3	240	1	12
d	4	240	3	12
e	5	280	1	3
f	6	280	3	3
g	7	280	1	12
h	8	280	3	12

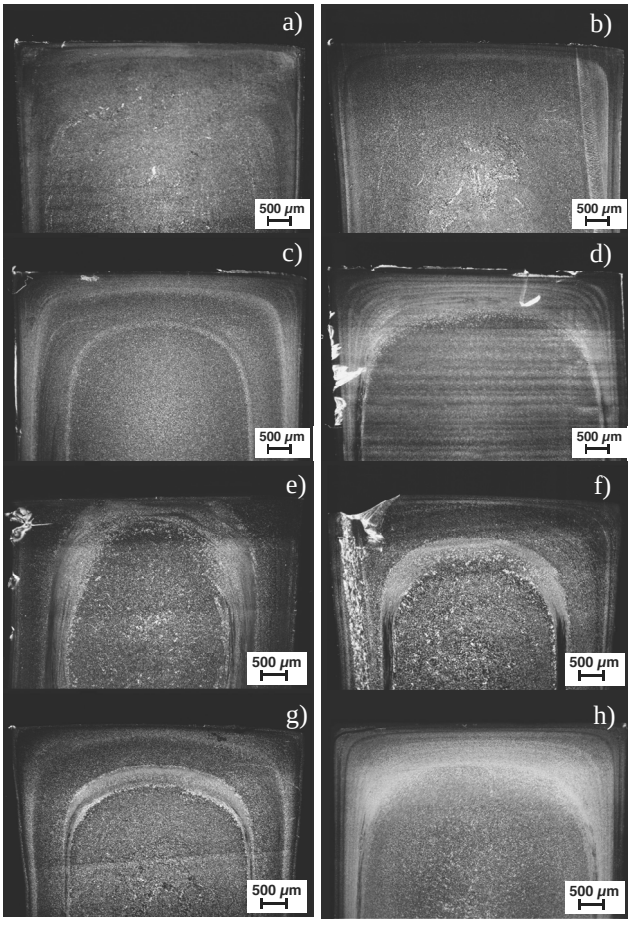

Fig. 24. Cross section of the neat PP specimens performed by N-CIM under different conditions accordingly to Table 9

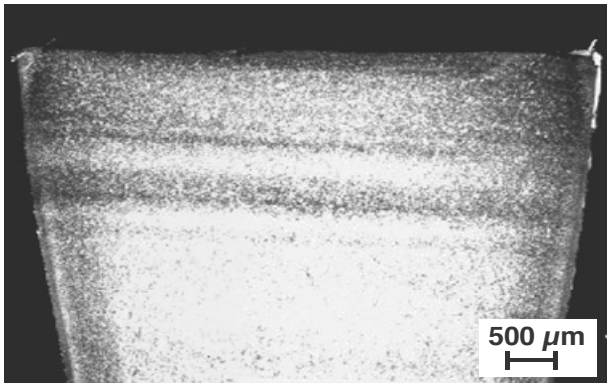

Fig. 25. Cross section of the PP/MMT 0.5% specimen performed by CIM in 240°C

Nanocomposites with 0.5% contribution of MMT particles, processed by CIM under low and high temperature, contain similar structure to neat PP, obtained under same condition (Figs. 25, 26). Thickness of the skin in these specimens reaches 110 microns. Forces, accompanying polymer melt redrawing during N-CIM process, formed multilayer zone, with the average layer thickness of 220 μm, for set 3, 4, 7, 8, where stroke number was set at maximum level (Fig. 27 c, d, g, h), and within them especially 4 and 8 (Fig. 27 d, h), equal to maxims of St and Sn.

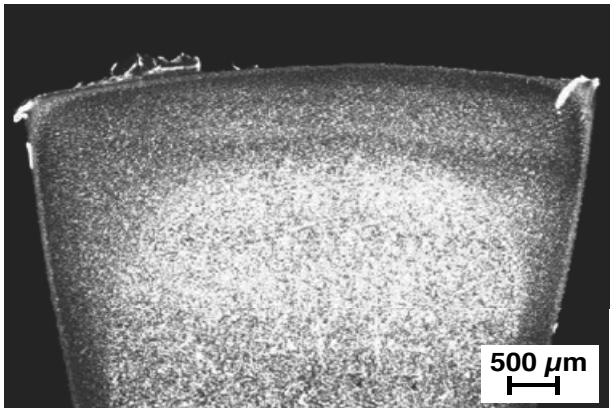

Fig. 26. Cross section of the PP/MMT 0.5% specimen performed by CIM in 280°C

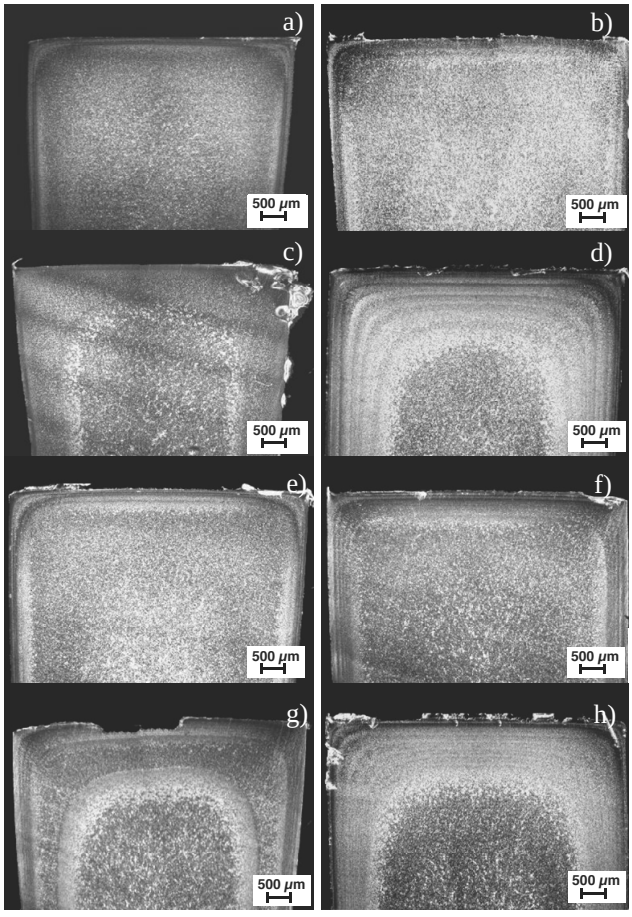

Fig. 27. Cross section of the PP/MMT 0.5% specimens performed by N-CIM under different conditions accordingly to Table 9

Increment of MMT contribution to 1% and use of CIM process, decides on skin forming with thickness 110 and 130 μm for low and high melt temperature and core occupies 94 and 95% respectively (Fig. 28, 29).

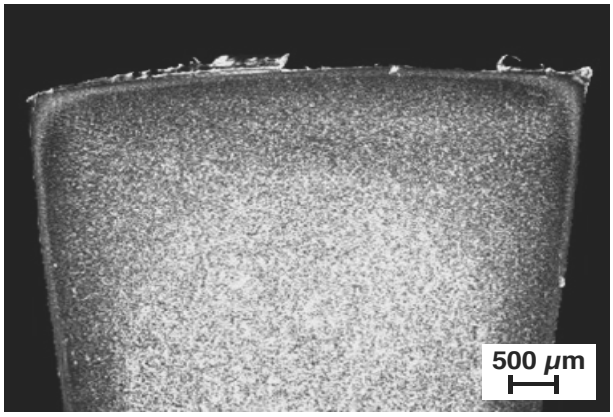

Fig. 28. Cross section of the PP/MMT 1% specimen performed by CIM in 240°C

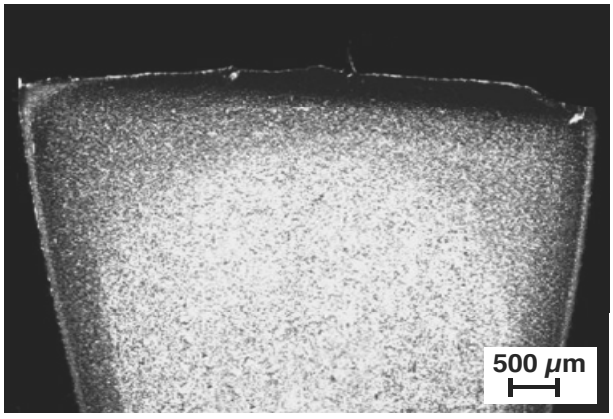

Fig. 29. Cross section of the PP/MMT 1% specimen performed by CIM in 240°C

Contribution of shear zone increases together with increment of St and Sn after use of N-CIM process, for lowTm (set 1, 2, 3, 4) (Fig. 30 a, b, c, d) and for high Tm (set 5, 6, 7, 8) (Fig. 30 e, f, g, h).

CIM process always creates core/skin structure with similar ratio of core and skin, independently of MMT contents in nanocomposite (Fig. 31). Addition of 10 wt% of MMT to polypropylene facilitates creation of agglomerates, owning to over saturation of the matrix by nanoparticles. Agglomerates are not enough solid and during cracking they will not block and retard crack propagation, so they are undesirable in the structure, weakening the material.

Volume of multilayered zones increases for nanocomposites with 3 and 5% of MMT, accordingly to increment of stroke numbers for both melt temperatures (Fig. 32, 33). For special consideration deserves nanocomposite PP/MMT 3% with a most developed structure, especially for specimens performed by N-CIM with set 4 and 8.

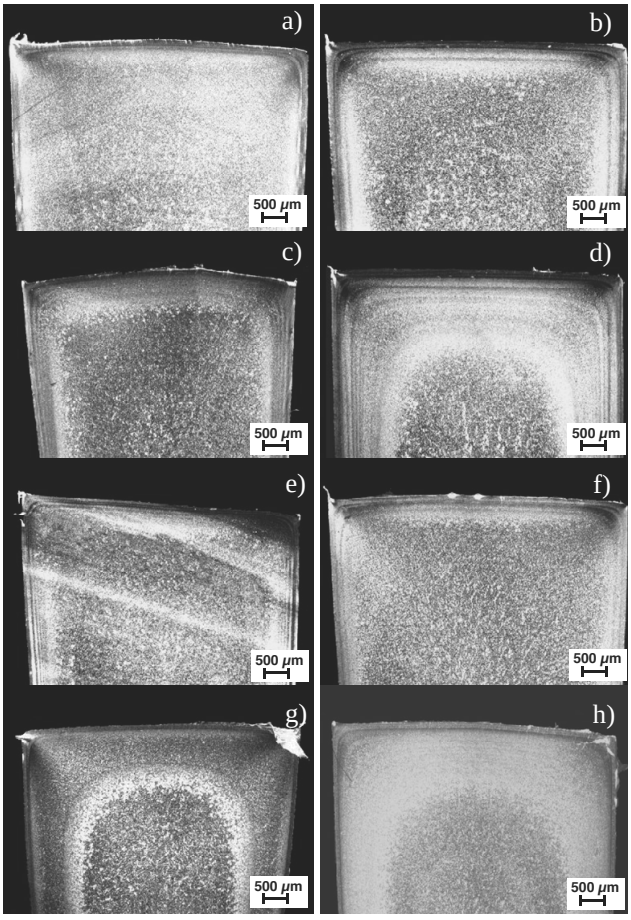

Fig. 30. Cross section of the PP/MMT 1% specimens performed by N-CIM under different conditions accordingly to Table 9

N-CIM process, thanks to high shear rates, shatters agglomerates of MMT in the structure; however some of them are visible at micro level (Fig. 34). Equally as in the case of other nanocomposites, N-CIM process induce creation of layers and mostly developed structure was obtained for PP/MMT 10% performed by set 4, 5 and 8 (Figs. 34 d, e, h).

Observations of fracture surfaces on scanning electron microscopy revealed plastic character of destruction of the specimens of pure polypropylene performed by CIM (Fig. 35) and N-CIM (Fig. 36).

Addition of 1% of nanoparticles didn't change the plastic character of the fracture, for specimens, processed both CIM (Fig. 37) and N-CIM (Fig. 38) technology.

The tendency of plastic character of fracture is maintained also for nanocomposites with 3 and 5% of nanofiller, namely PP/MMT 3% and PP/MMT 5%. Change in energy absorption appears for nanocomposite PP/MMT 10%. Brittle fracture connected with low energy absorption arises from over-richness of particles inside matrix and formation of agglomerates for both specimens performed by CIM (Fig. 39) and N-CIM (Fig. 40).

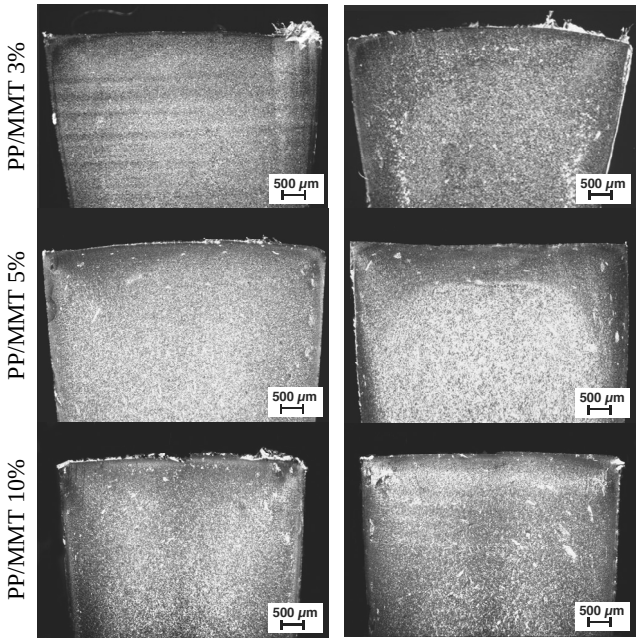

Fig. 31. Cross section of nanocomposites performed by CIM in 240°C (left column) and 280°C (right column)

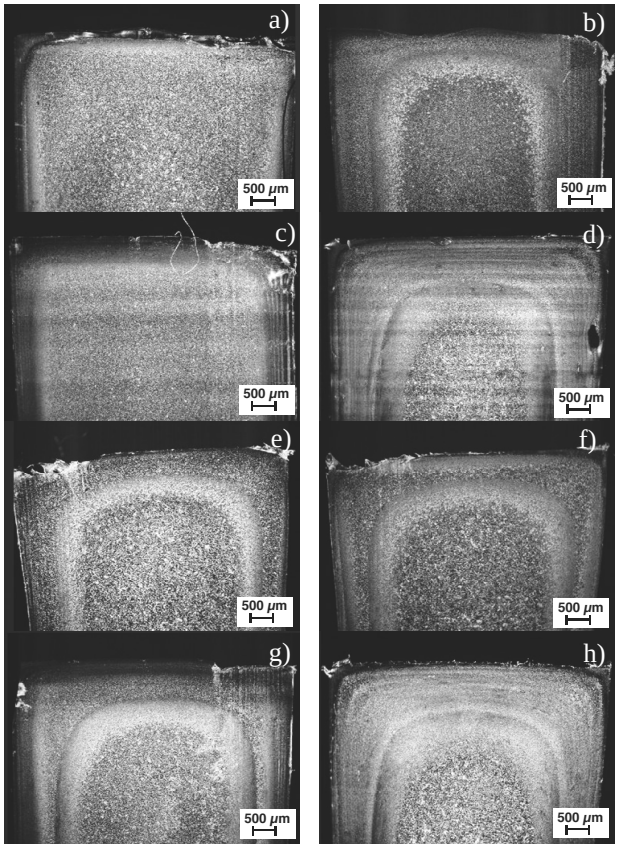

Fig. 32. Cross section of the PP/MMT 3% specimens performed by N-CIM under different conditions accordingly to Table 9

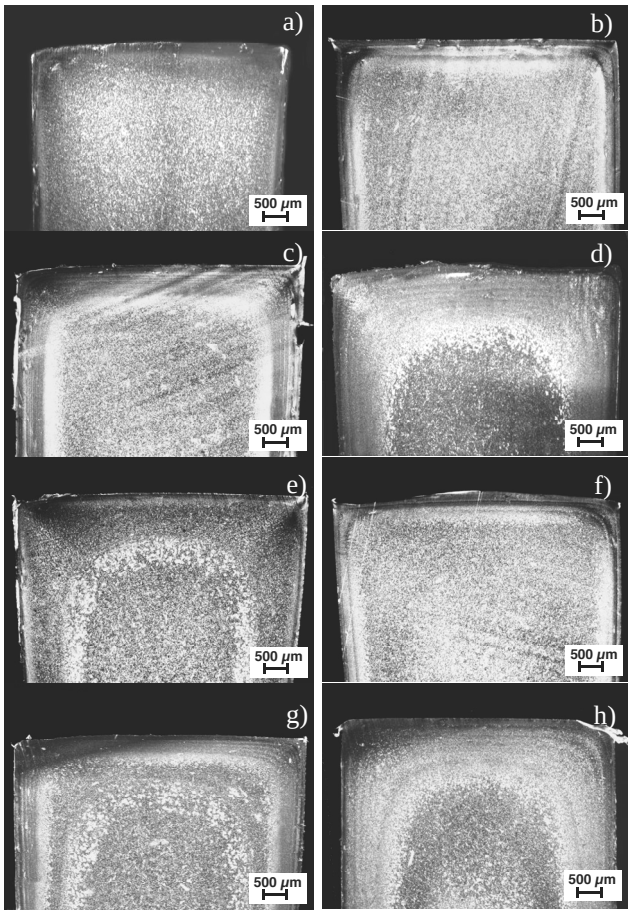

Fig. 33. Cross section of the PP/MMT 5% specimens performed by N-CIM under different conditions accordingly to Table 9

Scanning micrographs of the fracture surfaces of the specimens could bring better look on the differences between the core, shear zone and outer skin energy absorption, by evaluation of the level of the roughness or smoothness of the surface or by calculating stress whitening area, which appears after fracture of polymeric materials. Further work in this direction can be done.

Confirmation of MMT particles inside polypropylene matrix was confirmed by energy dispersive spectrometry on SEM (Figs. 41, 42).

Higher magnification, obtained on SEM, approached particle dispersion and unidirectional orientation. For specimens of PP/MMT 3% performed by CIM, can be reported good dispersion inside polypropylene matrix with visible tendency to formation of montmorillonite agglomerates, with size of 5 μm, for both processing temperatures (Figs. 41, 42).

Application of N-CIM technology induced high shear rates, during solidification phase of polymer and splatted agglomerates, assuring intercalation of particles. Best intercalation was achieved for nanocomposite PP/MMT 3%, processed under high level of St and Sn values (set 4 and 8) for both temperatures (Fig. 43, 44).

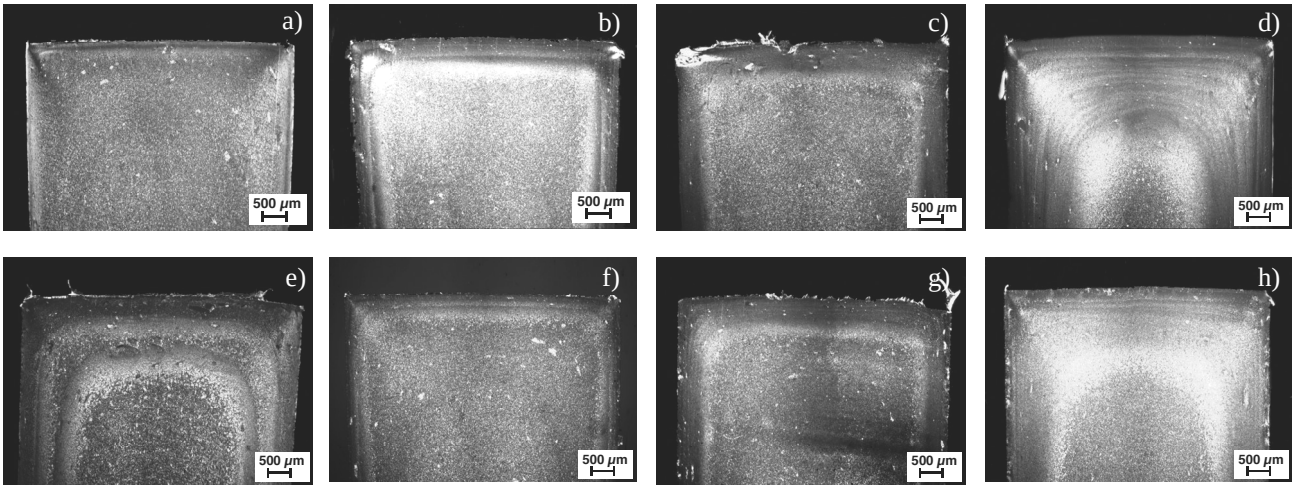

Fig. 34. Cross section of the PP/MMT 10% specimens performed by N-CIM under different conditions accordingly to Table 9

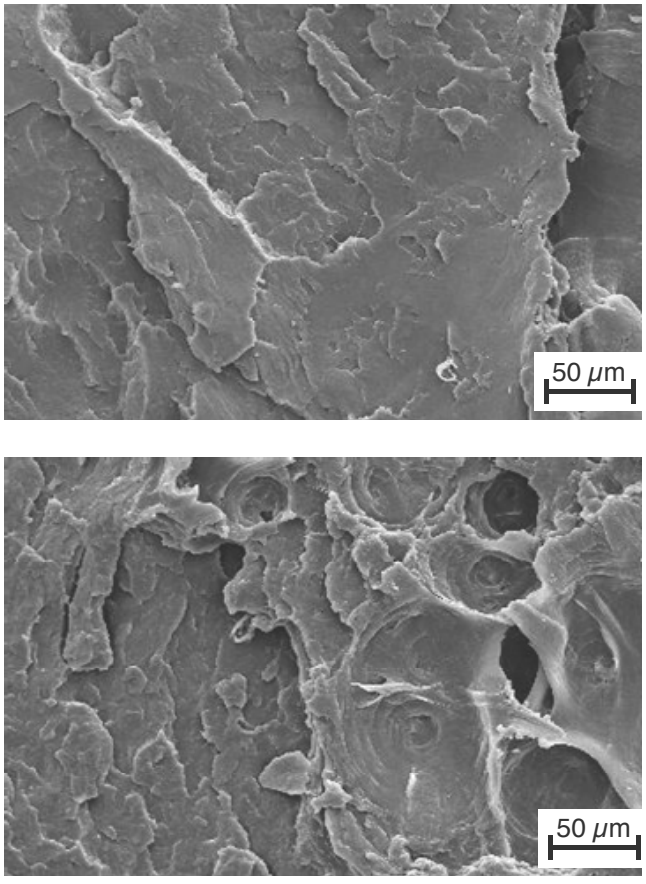

Fig. 35. Cross section of the neat PP specimens performed by CIM in 240°C (top figure) and 280°C (bottom figure)

Orientation of MMT galleries is in accordance to polymer flow during alternating extension and retraction of the melt in the mould cavity, has been achieved (Figs. 45-47).

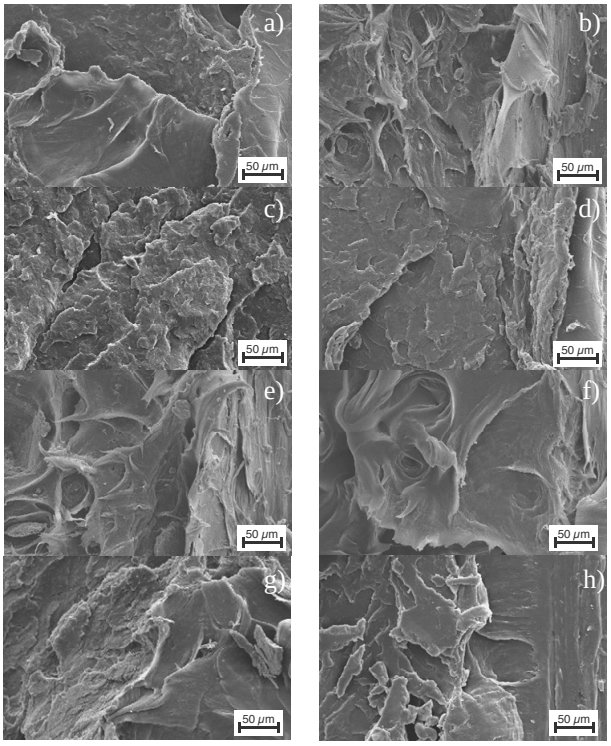

Fig. 36. Cross section of the neat PP specimens performed by N-CIM under different conditions accordingly to Table 9

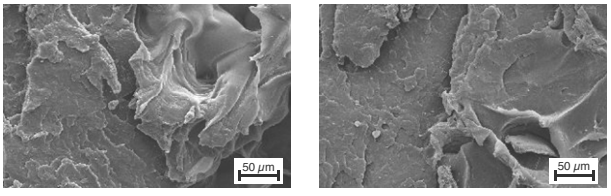

Fig. 37. Cross section of the PP/MMT 1% specimens performed by CIM in 240°C (left figure) and 280°C (right figure)

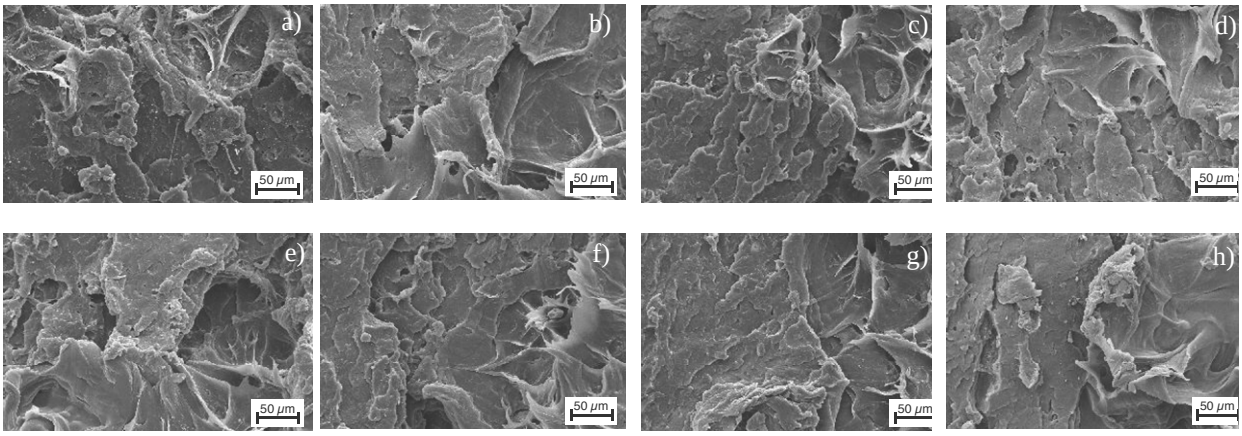

Fig. 38. Cross section of the PP/MMT 1% specimens performed by N-CIM under different conditions accordingly to Table 9

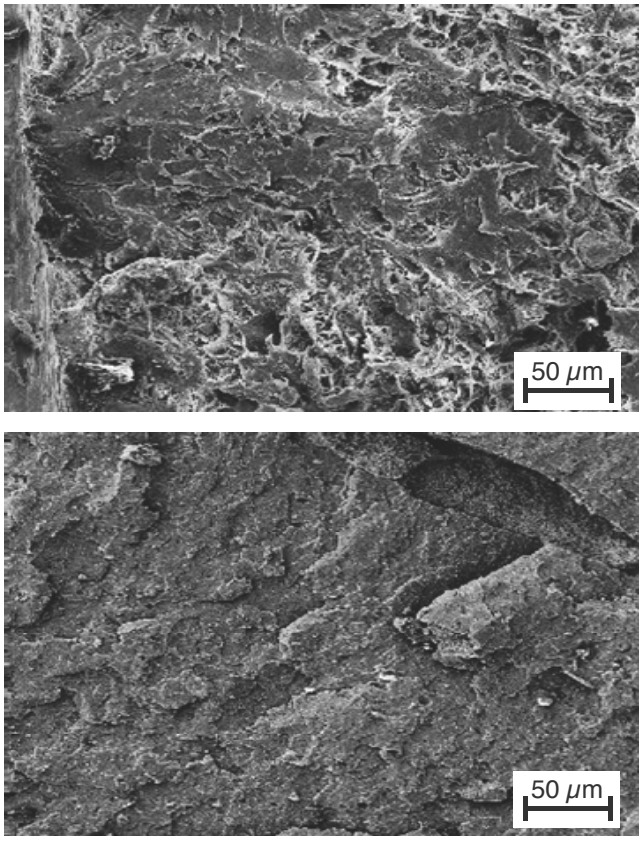

Fig. 39. Cross section of the PP/MMT 10% specimens performed by CIM in 240°C (top figure) and 280°C (bottom figure)

Confirmation of intercalation of MMT particles and interplanar distance between particular platelets of MMT gallery was confirmed by transmission electron microscopy with computer aided image analysis. The distance between plates is equal to 2.7 nm (Figs. 48-51).

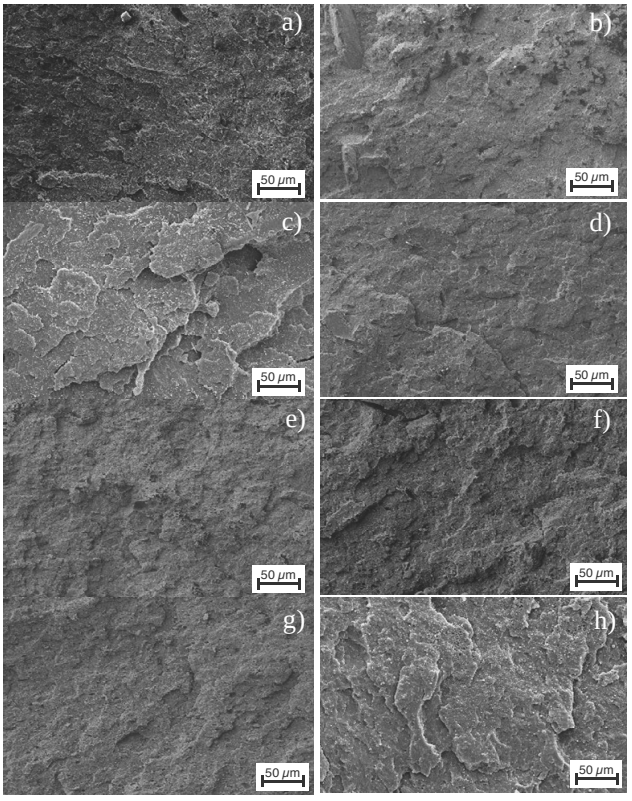

Fig. 40. Cross section of the PP/MMT 10% specimens performed by N-CIM under different conditions accordingly to Table 9

Nanosized particles influence morphology and it's confirmed also their affection on stiffness and toughness of obtained specimens, and these properties increase together with increment of nanofiller content up to 5 wt%. Results of neat polypropylene bending test are presented below (Table 10, Fig. 52). These results are served as the primary results, to whose refer subsequent results of nanocomposites testing.

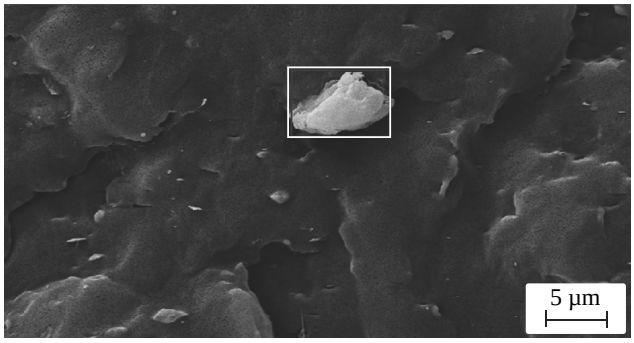

Fig. 41. MMT agglomerate inside polypropylene matrix

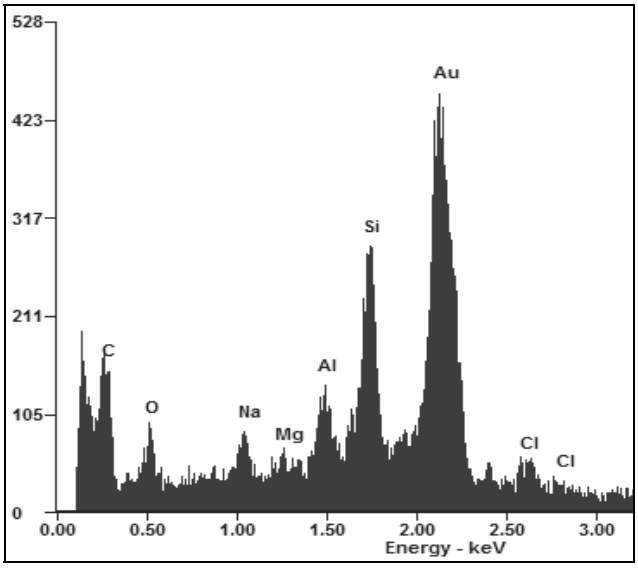

Fig. 42. Elements detected in MMT agglomerate by energy dispersive spectrometry

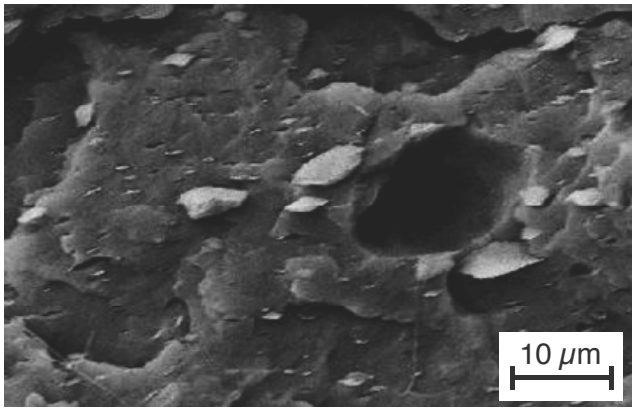

Fig. 43. Cross section of the PP/MMT 3% specimen performed by CIM in 240°C; visible particular agglomerates of MMT platelets

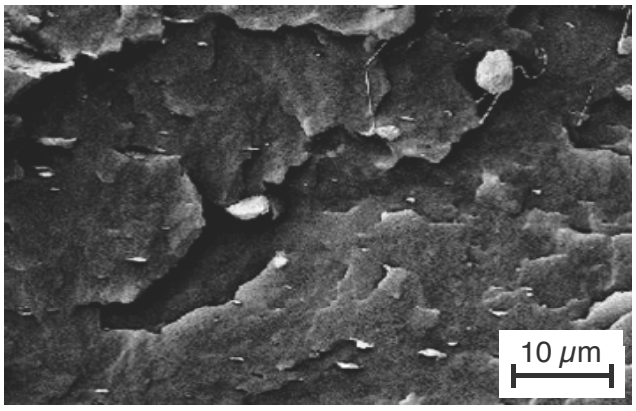

Fig. 44. Cross section of the PP/MMT 3% specimen performed by CIM in 280°C; visible particular agglomerates of MMT platelets

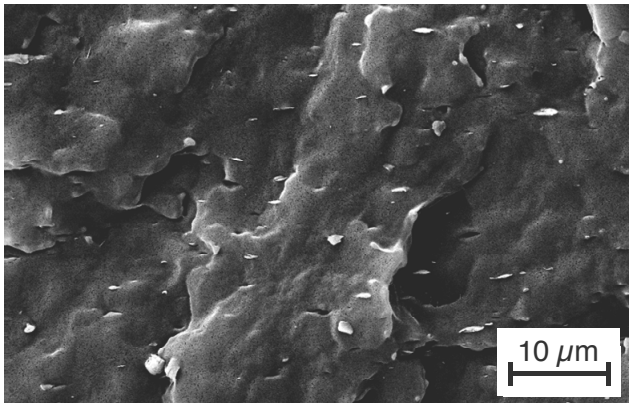

Fig. 45. Cross section of the PP/MMT 3% specimen performed by N-CIM in 240°C under condition equal to maximum St and Sn (set 4 accordingly to Table 9); absence of huge MMT agglomerates

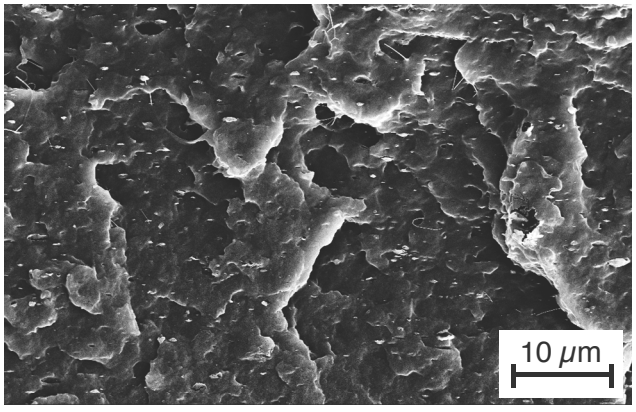

Fig. 46. Cross section of the PP/MMT 3% specimen performed by N-CIM in 280°C under condition equal to maximum St and Sn (set 8 accordingly to Table 9); absence of huge MMT agglomerates

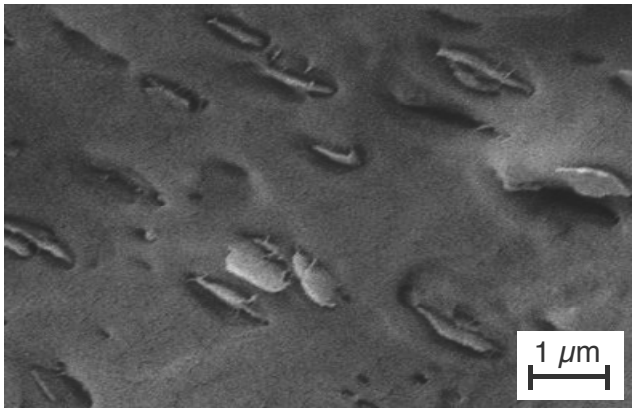

Fig. 47. Cross section of the PP/MMT 3% specimen performed by N-CIM in 280°C under condition equal to maximum St and Sn (set 8 accordingly to Table 9)

Fig. 48. Intercalation of MMT galleries approved by transmission electron microscopy

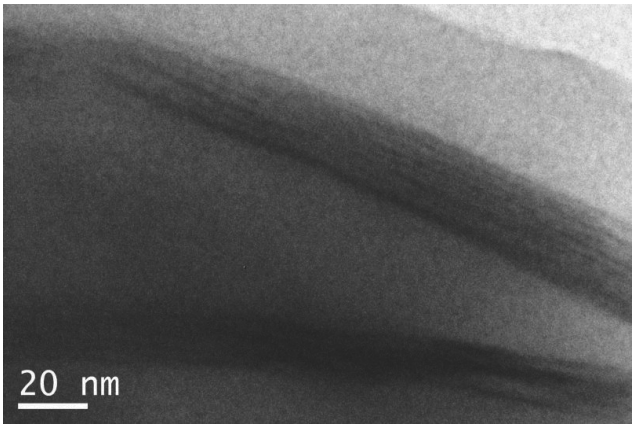

Fig. 49. Intercalation of MMT galleries approved by transmission electron microscopy

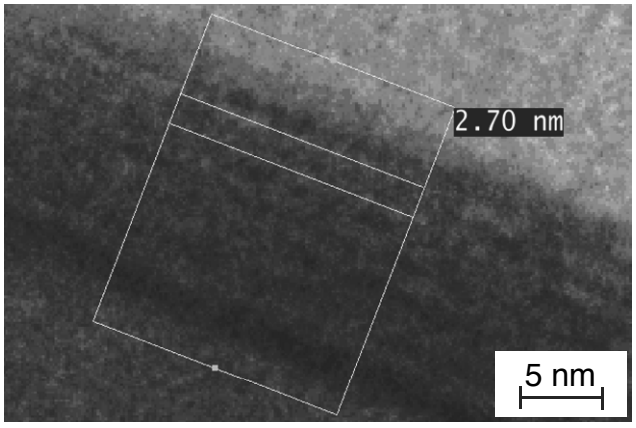

Fig. 50. Intercalation of MMT galleries approved by transmission electron microscopy

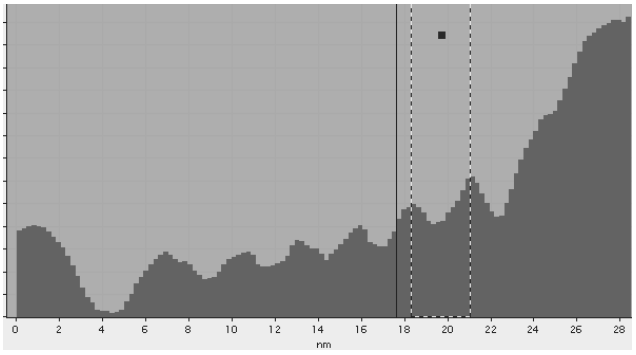

Fig. 51. Profile of MMT gallery with visible interplanar distances

Table 10.
Flexural strength of polypropylene specimens, MPa

Process	Set	Statistical values		
		Arithmetic average σ_{max}, MPa	Standard deviation	Confidence interval min-max
CIM	1	36.40	1.66	36.04-37.13
	2	38.94	1.78	38.55-39.72
N-CIM	1	29.74	1.36	29.44-30.33
	2	30.79	1.40	30.48-31.41
	3	34.90	1.59	34.55-35.60
	4	47.56	2.17	47.09-48.51
	5	22.64	1.03	22.41-23.09
	6	26.14	1.19	25.88-26.67
	7	37.78	1.72	37.41-38.54
	8	42.45	1.94	42.02-43.30

The testing of strength properties were carried out in order to determine flexural strength, examine and compare absorbed energy by the action of lateral force on the sample as a function of contribution of nanoparticles and changes of the injection moulding process conditions.

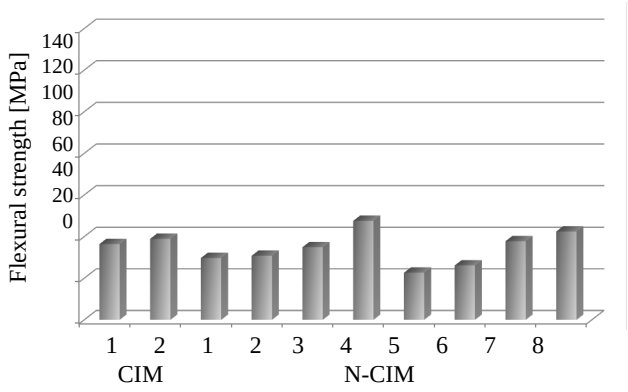

Fig. 52. Flexural strength of polypropylene specimens performed by CIM and N-CIM

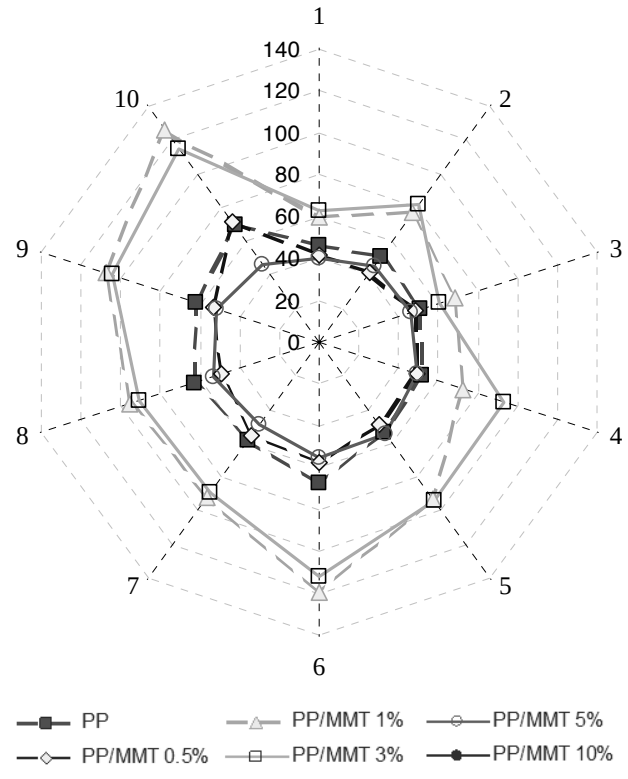

Fig. 53. Collation of results of polypropylene and nanocomposites' flexural strength performed by CIM (1 and 2) and N-CIM (3-10), MPa

For all conditions increment of MMT improved mechanical performance. Best improvement was reported for specimens of PP/MMT 3%, obtained in higher temperature, performed by N-CIM process with maximum St-Sn values, reaching value of 125 MPa, which is quasi 3 times more, comparing to neat PP performed in the same condition (42 MPa) and more then 3 times bigger than value (38 MPa), originating from neat PP performed by CIM (Fig. 53).

Flexural modulus doesn't represent huge divergence in results including all materials performed by CIM and N-CIM processes. However, similarly as in the case of flexural strength, neat PP represents lowest values and PP/MMT 3% and PP/MMT 5% highest ones (Fig. 54).

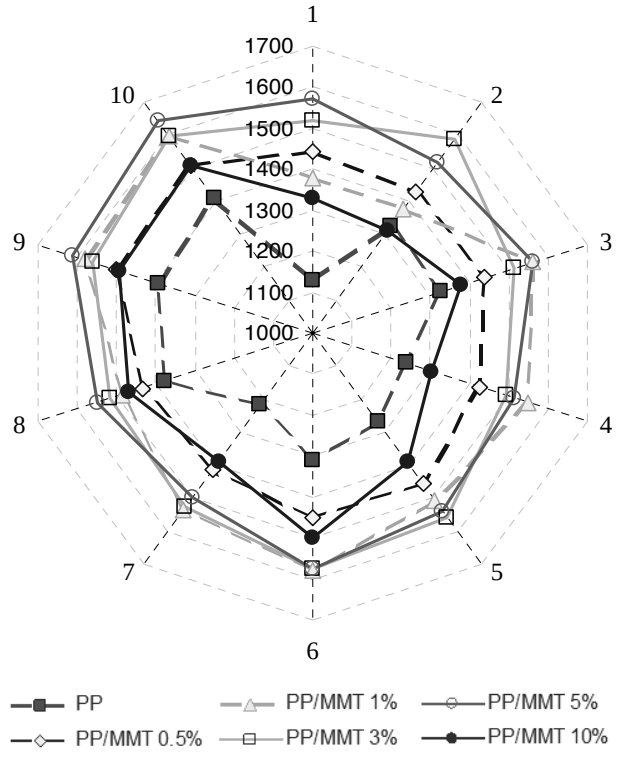

Fig. 54. Collation of results of polypropylene and nanocomposites' flexural modulus, performed by CIM (1 and 2) and N-CIM (3-10), MPa

Optimization of processing, aimed to design and select the most favourable variables, including injection moulding temperature, stroke time and stroke number, determining the properties, is a key issue. The graphs below show the contribution of variable parameters on flexural strength of tested materials. Flexural strength is mainly controlled by stroke number for PP, PP/MMT 3% and PP/MMT 5% (Figs. 55, 56, 57).

For the nanocomposite PP/MMT 0.5% flexural strength is mainy controlled simultaneously by melt temperature and stroke number (42.7% and 41.5% respectively (Fig. 58).

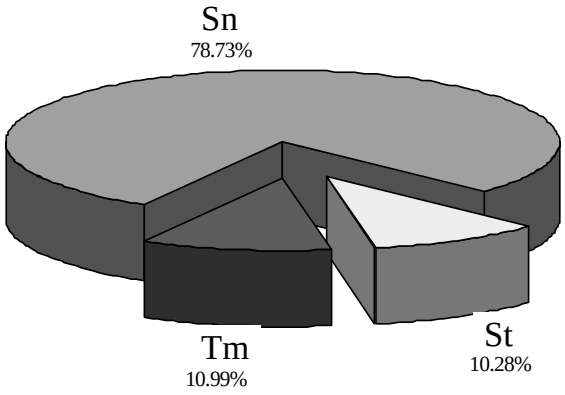

Fig. 55. Contribution of N-CIM processing parameters on flexural strength of PP; Tm – melt temperature, St – stroke time, Sn – stroke number

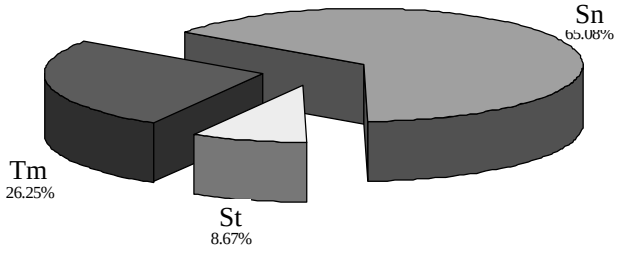

Fig. 56. Contribution of N-CIM processing parameters on flexural strength of PP/MMT 3%; Tm – melt temperature, St – stroke time, Sn – stroke number

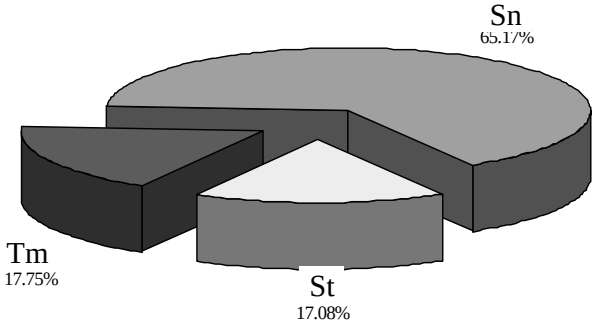

Fig. 57. Contribution of N-CIM processing parameters on flexural strength of PP/MMT 5%; Tm – melt temperature, St – stroke time, Sn – stroke number

Nanocomposite's PP/MMT 1% flexural strength is controlled simultaneously by interaction between melt temperature and stroke time (32.8%) and by particular factors, namely stroke number (28.9%) and melt temperature (25.8%) (Fig. 59).

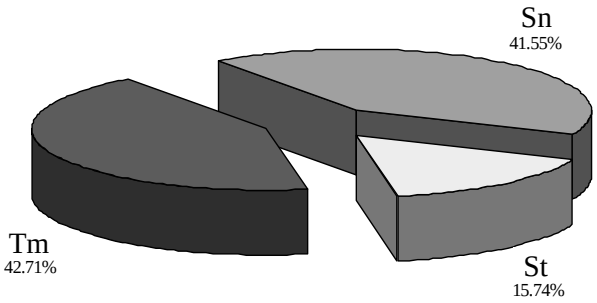

Fig. 58. Contribution of N-CIM processing parameters on flexural strength of PP/MMT 0,5%; Tm – melt temperature, St – stroke time, Sn – stroke number

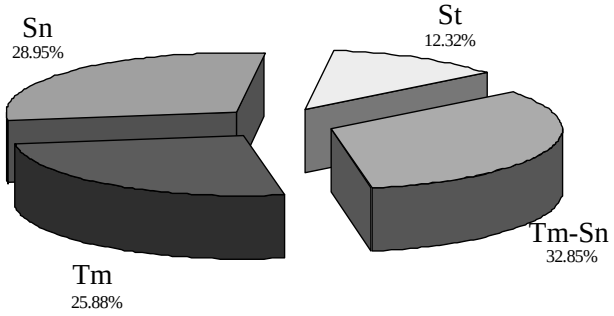

Fig. 59. Contribution of N-CIM processing parameters on flexural strength of PP/MMT 1%; Tm – melt temperature, St – stroke time, Sn – stroke number

Research carried out using synchrotron radiation were the basis of material and structure characterization, performed to verify the degree of crystallinity of the polymer matrix nanocomposites and to verify the presence of crystallographic planes (Figs. 60, 61). Research confirmed presence of crystallographic planes: (110), (040), (130), (111), (041) with the corresponding values of interplanar distances, d, calculated from the equation of Braggs' low with $\lambda = 0.15$ (Table 11, Figs. 60, 61).

For the modified montmorillonite, where an exchange of sodium, calcium and potassium ions on alkylammonium, ions increases the distance between the MMT plates to about 2.6 nm, which is approved by research. This modification is necessary due to the hydrophilic nature of the montmorillonite and the poor miscibility with the polymer, and leads to better wetting and dispersion of platelets in the matrix polymer.

Structural analysis by wide angle X-ray diffraction confirms the presence of characteristic structure for α isotactic polypropylene, in which exist crystals with monoclinic unit cell of values of angles $\alpha = \gamma = 90\ ^\circ$ and $\beta = 99.2\ ^\circ$ and distances a = 0.665 nm, b = 2.096 nm and c = 0.650 nm.

Table 11.
Interplanar distances, d, calculated from the equation of Braggs' low

Crystallo-graphic plane	θ angle	Interplanar distances, d $d = \lambda/(2\sin\theta)$, $\lambda = 0.15$					
		PP	PP/MMT				
			0.5%	1%	3%	5%	10%
(110)	7.0535	0.611	0.606	0.609	0.613	0.610	0.610
(040)	8.3817	0.515	0.511	0.513	0.517	0.513	0.513
(130)	9.1985	0.469	0.466	0.469	0.471	0.469	0.469
(111)	10.4811	0.412	0.406	0.409	0.412	0.412	0.413
(041)	10.8389	0.399	0.395	0.397	0.400	0.398	0.399

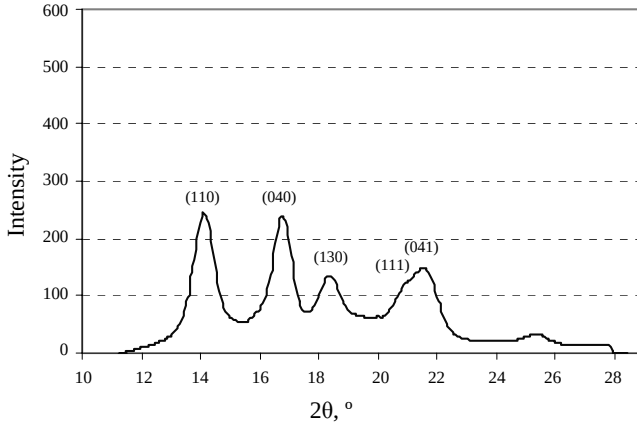

Fig. 60. Diffractogram of polypropylene specimens containing α crystals, performed by N-CIM with maximum Tm, St and Sn values (set 8 accordingly to Table 9); main peaks are marked with Miller indices of corresponding crystallographic planes

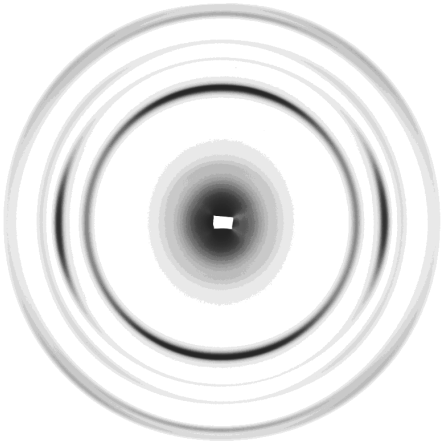

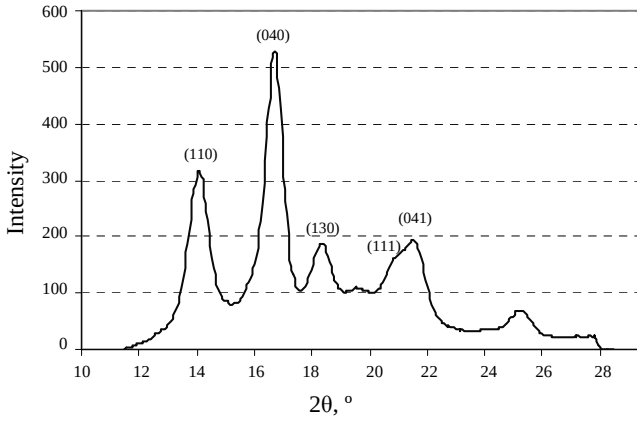

Fig. 61. Diffractogram of PP/MMT 3% specimens containing α crystals, performed by N-CIM with max Tm, St and Sn values

Addition of nanoparticles increased temperature of crystallization for specimens performed by CIM up to 5 wt% of MMT content and slightly decrease for PP/MMT 10% (Fig. 62). Application of N-CIM process creates dependence, where temperature of crystallization decreases together with increment of MMT content (Fig. 63).

Degree of crystallinity increases after addition of nano-particles and then slowly decreases together with increment of nanofiller for specimens performed by CIM (Fig. 64). Similar behaviour have specimens performed by N-CIM (Fig. 65).

Analysis of variance in the given range of values of minimum and maximum values corresponding to the processing conditions, accordingly to design of experiment, gives possibility to predict increment of flexural strength through increasing or decreasing of processing parameters of N-CIM technology, namely Tm, St and Sn, in the form of single actions and interactions between these parameters. Interaction occurs when the response is different and depends on the settings of two factors, and the graph is then interpreted as a two-level interaction, and two lines of two values are not parallel to each other, which means, that the effect of one factor depends on the level of the second one.

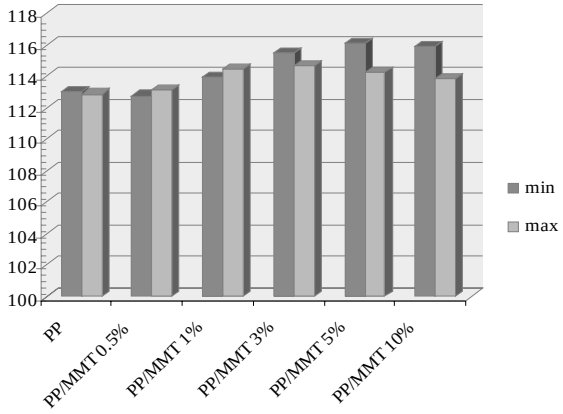

Fig. 62. Summary of the temperature of crystallization of polypropylene and nanocomposites performed by CIM with minimum and maximum values of Tm

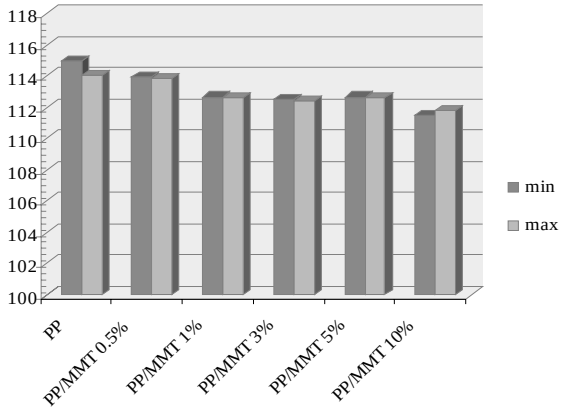

Fig. 63. Summary of the temperature of crystallization of polypropylene and nanocomposites performed by N-CIM with minimum and maximum values of Tm, St and Sn (set 1 and 8 accordingly to Table 9)

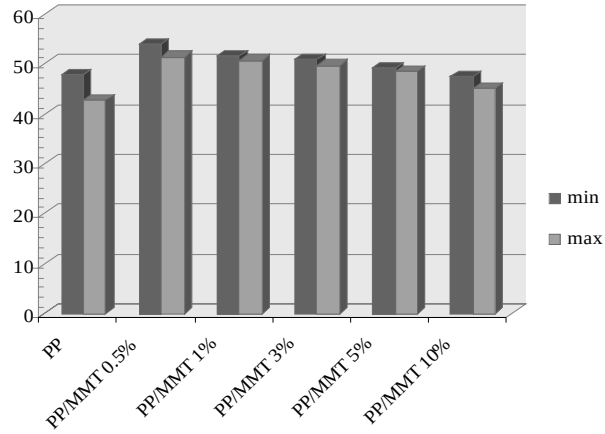

Fig. 64. Summary of the degree of crystallinity of polypropylene and nanocomposites performed by CIM with minimum and maximum values of Tm

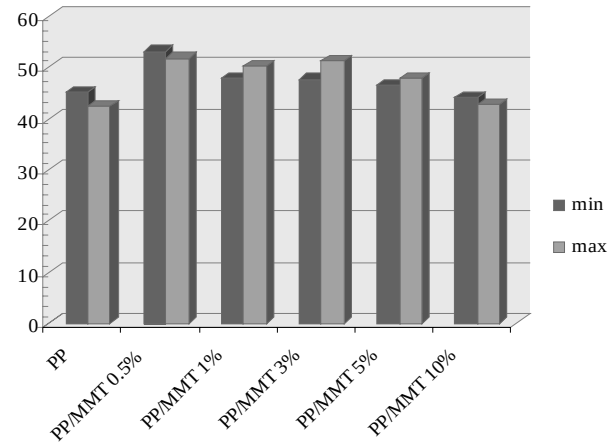

Fig. 65. Summary of degree of crystallinity of polypropylene and nanocomposites performed by N-CIM with minimum and maximum values of Tm, St and Sn (set 1 and 8 accordingly to Table 9)

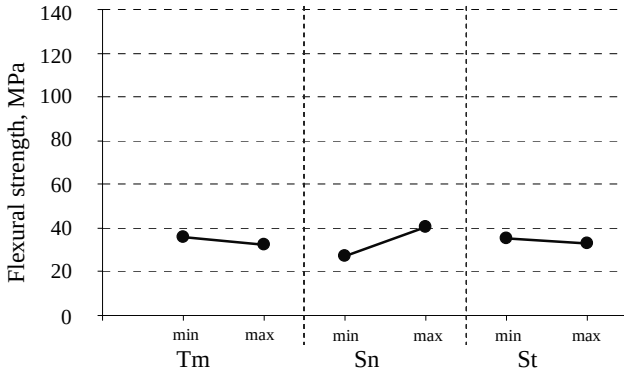

Fig. 66. Analysis of variance for nanocomposite PP, describes influence of increment of processing parameters from minimum to maximum value, according to previously desighned plan, on flexural strength; min/max value: Tm = 240ºC/280ºC, Sn = 3/12, St = 1/3s

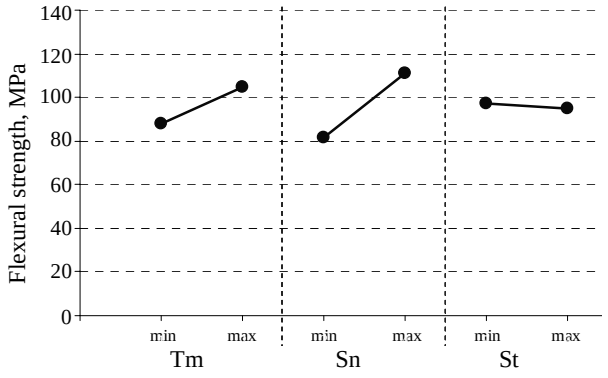

Fig. 67. Analysis of variance for nanocomposite PP/MMT 3%, describes influence of increment of processing parameters from minimum to maximum value, according to previously desighned plan, on flexural strength; min/max value: Tm= 240ºC/280ºC, Sn=3/12, St=1/3s

Basing on obtained flexural strength results and analysis of variance for neat PP can be observed, that increment of stroke number and decrement of melt temperature and stroke time reinforce material (Fig. 66). In the case of nanocomposite PP/MMT 3% increment of melt temperature and stroke number will affect in increment of flexural strength while increment of stroke time will weaken the material (Fig. 67).

4. Summary

Comparison of structural and mechanical properties nanocomposites processed in many diversified ways with CIM and N-CIM process, brought complex information of their behaviour. Addition of nanoparticles improved strength of composites and thanks to advanced processing technology has been obtained almost triple enhancement of compositions, satisfying initial assumption of this work. Design of experiment schedule was helpful in optimizing average response values and also in minimizing effects of variability on process assuring robust design. Nanocomposites significantly react on N-CIM technique providing to well reinforcement of structure and to multilayer zone.

MMT particles considerably increase absorption of energy in mechanical tests. Level of absorbed energy required to bend the specimens during flexural test increases dramatically after reinforcing the material with MMT nanoparticles. Internally located particles in the matrix prolong the crack propagation. Slalom-like crack propagation comes slower in the time by reason of bypassing parallely oriented lamella-like nanoclay tactoids.

It can be reported that high shear rates supports in inducing a thicker multilayered, highly oriented shear zone, especially visible in the case of PP/MMT 3% processed with maximum Tm, St and Sn (Fig. 32 h), uniform distribution of nano plates inside material in shear zone (Fig. 46) and play meaningful role in improving flexural strength (Fig. 53).

The N-CIM process created multilayer structure. Specimens performed by CIM contain big core, occupying 90% of specimen, which is almost double comparing to structure of specimens performed by N-CIM, where core occupies 52%. For he rest of specimen consist skin (in the case of CIM) and shear zone/skin structure (in the case of N-CIM). This indicates, that N-CIM process creates structure with developed shear zone four times bigger than skin, created in conventional injection moulding (48% to 10% ratio).

Melt temperature, stroke time and stroke number are determinants of the flexural strength in the process and their dependences, basing on analysis of variance, may improve or predict new properties.

MMT agglomerates can be easily splitten, due to high shear rates in the flow orientation induced by strokes, so the N-CIM process can be efficiently used to obtain high performance nanocomposites without pre-treatment. Creation of thin layers by this process is the significant step in advancement of polymer composites and nanocomposites, simultaneously giving ability of morphology control and project materials with expected properties.

References

[1] R.F. Gibson, A review of recent research on mechanics of multifunctional composite materials and structures, Composite Structures 92/12 (2010) 2793-2810.

[2] E.J. Barbero, Introduction to Composite Materials Design, CRC Press, 2010.

[3] D.V. Rosato, M.G. Rosato, Injection molding handbook Third Edition, Kluwer Academic Publishers, 2000.

[4] S.S. Ray, M. Okamoto, Polymer/layered silicate nanocomposites: a review from preparation to processing, Progress in Polymer Science 28 (2003) 1539-1641.

[5] L.A. Dobrzański, M. Drak, Structure and properties of composite materials with polymer reinforced Nd-Fe-B hard magnetic materials, Journal of Materials Processing Technology 157-158 (2004) 650-657.

[6] E.P. Giannelis, Polymer Layered Silicate Nanocomposites, Advanced Materials 8/1 (1996) 29-35.

[7] J.C. Viana, N. Billon, A.M. Cunha, The Thermo-mechanical Environment and the Mechanical Properties of Injection Moldings, Polymer Engineering and Science 44/8 (2003) 1522-1533.

[8] D.B. Tchalamov, J.C. Viana, A.M. Cunha, Mechanical Properties of Two Component Injection Molded Parts, Proceedings of the SPE ANTEC, San Francisco, CA, USA, 2002.

[9] L. Cížek, M. Greger, L. Pawlica, L.A. Dobrzański, T. Tański, Study of selected properties of magnesium alloy AZ91 after heat treatment and forming, Journal of Materials Processing Technology 157-158 (2004) 466-471.

[10] A. Kumar, R.K. Gupta, Fundamentals of polymer engineering, Marcel Dekker, 2003.

[11] L.A. Dobrzański, W. Sitek, Application of a neural network in modelling of hardenability of constructional steels, Journal of Materials Processing Technology 78/1-3 (1998) 59-66.

[12] L.A. Dobrzański, M. Kowalski, J. Madejski, Methodology of the mechanical properties prediction for the metallurgical products from the engineering steels using the Artificial Intelligence methods, Journal of Materials and Processing Technology 164 (2004) 1500-1509.

[13] A. Grajcar, W. Borek, Thermo-mechanical processing of high-manganese austenitic TWIP-type steels, Archives of Civil and Mechanical Engineering 8/4 (2008) 29-38.

[14] T. Jaruga, E. Bociąga, Structure of polypropylene parts from multicavity injection mould, Archives of Materials Science and Engineering 28/7 (2007) 429-432.

[15] T. Jaruga, Dynamic mechanical properties of parts from multicavity injection mould, Journal of Achievements in Materials and Manufacturing Engineering 23/2 (2007) 83-86.

[16] M. Bilewicz, J.C. Viana, A.M. Cunha, L.A. Dobrzański, Polymer composite strengthening by developed injection moulding technique, Archives of Material Science and Engineering 30/2 (2008) 69-72.

[17] I.A. Mandzyuk, V.V. Romanuke, Rheometric research of polypropylene Licocene PP2602 melts, Archives of Materials Science and Engineering 50/1 (2011) 31-35.

[18] K. Gołombek, L.A. Dobrzański, M. Soković, Properties of the wear resistant coatings deposited on the cemented carbides substrates in the cathodic arc evaporation process,

Journal of Materials and Processing Technology 157 (2004) 341-347.
[19] M. Bilewicz, J.C. Viana, A.M. Cunha, Non-conventional Injection Moulding of a PP/PC-ABS Blend Materials Science Forum 514-516 (2006) 858-862.
[20] L.A. Dobrzański, J. Mazurkiewicz, E. Hajduczek, Effect of thermal treatment on structure of newly developed 47CrMoWVTiCeZr16-26-8 hot-work tool steel, Journal of Materials Processing Technology 157-158 (2004) 472-484.
[21] M. Bilewicz, J.C. Viana, A.M. Cunha, L.A. Dobrzański, Morphology diversity and mechanical response of injection moulded polymer composites and polymer-polymer composites, Journal of Achievements in Materials and Manufacturing Engineering 15 (2006) 159-165.
[22] L.A. Dobrzański, A. Zarychta, M. Ligarski, High-speed steels with addition of niobium or titanium, Journal of Materials Processing Technology 63/1-3 (1997) 531-541.
[23] D.D.J. Rousseaux, N. Sallem-Idrissi, A.C. Baudouin, J. Devaux, P. Godard, J. Marchand-Brynaert, Water-assisted extrusion of polypropylene/clay nanocomposites: A comprehensive study, Polymer 52/2 (2011) 443-451.
[24] B. Hajduk, P. Jarka, J. Weszka, M. Bruma, J. Jurusik, M. Chwastek, D. Mańkowski, Comparing of optical properties and morphology of polyoxadiazoles with CF, Journal of Achievements in Materials and Manufacturing Engineering 40/1 (2010) 7-14.
[25] M. Bilewicz, J.C. Viana, L.A. Dobrzański, Self-reinforced polymer-polymer composites, Journal of Achievements in Materials and Manufacturing Engineering 24/2 (2007) 43-46.
[26] M. Bilewicz, J.C. Viana, L.A. Dobrzański, Development of microstructure affected by in-mould manipulation in polymer composites and nanocomposite, Journal of Achievements in Materials and Manufacturing Engineering 31/1 (2008) 71-76.
[27] L.A. Dobrzański, M. Król, M. Bilewicz, J.C. Viana, Microstructure and mechanical properties of Polypropylene/ Polycarbonate blends, Journal of Achievements in Materials and Manufacturing Engineering 27/1 (2008) 19-22.
[28] P. Gomez-Romero, C. Sanchez, Functional Hybrid Materials, John Wiley & Sons, 2006.
[29] S.K. Kumar, R. Krishnamoorti, Nanocomposites: Structure, Phase Behavior, and Properties, Annual Review of Chemical and Biomolecular Engineering 1 (2010) 37-58.
[30] L.A. Dobrzański, L.W. Żukowska, Properties of the multicomponent and gradient PVD coatings, Archives of Materials Science and Engineering 28/10 (2007) 621-624.
[31] L.A. Dobrzański, A. Tomiczek, B. Tomiczek, A. Ślawska-Waniewska, O. Iesenchuk, Polymer matrix composite materials reinforced by $Tb_{0.3}Dy_{0.7}Fe_{1.9}$ magnetostrictive particles, Journal of Achievements in Materials and Manufacturing Engineering 37/1 (2009) 16-23.
[32] G. Wróbel, S. Pawlak, The effect of fiber content on the ultrasonic wave velocity in glass/polyester composites, Journal of Achievements in Materials and Manufacturing Engineering 20 (2007) 295-298.
[33] G. Wróbel, S. Pawlak, A comparison study of the pulseecho and through-transmission ultrasonics in glass/epoxy composites, Journal of Achievements in Materials and Manufacturing Engineering 22/2 (2007) 51-54.
[34] T.G. Rochow, P.A. Tucker, Introduction to Microscopy by Means of Light, Electrons, X Rays or Acoustics, Springer, 1994.
[35] T. Jaruga, E. Bociąga, Crystallinity of parts from multicavity injection mould, Archives of Materials Science and Engineering 30/1 (2008) 53-56.
[36] P. Postawa, D. Kwiatkowski, E. Bociaga, Influence of the method of heating/cooling moulds on the properties of injection moulding parts, Archives of Materials Science and Engineering 31/2 (2008) 121-124.
[37] L. Čížek, L. Pawlica, R. Kocich, M. Janošec, T. Tański, M. Praźmowski, Structure and properties of Mg-Zr and Mg-Si alloys, Journal of Achievements in Materials and Manufacturing Engineering 27/2 (2008) 127-130.
[38] A. Shokuhfara, A. Zare-Shahabadib, A.A. Ataic, S. Ebrahimi-Nejada, M. Termeha, Predictive modeling of creep in polymer/layered silicate nanocomposites, Polymer Testing 31/2 (2012) 345-354.
[39] L.A. Dobrzański, K. Labisz, E. Jonda, Laser treatment of the surface layer of 32CrMoV12-28 and X40CrMoV5-1 steels, Journal of Achievements in Materials and Manufacturing Engineering 29/1 (2008) 63-70.
[40] L.A. Dobrzański, B. Tomiczek, M. Adamiak, Manufacturing of EN AW 6061 matrix composites reinforced by halloysite nanotubes, Journal of Achievements in Materials and Manufacturing Engineering 49/1 (2011) 82-89.
[41] M. Żenkiewicz, P. Rytlewski, K. Moraczewski, M. Stepczyńska, T. Karasiewicz, R. Malinowski, W. Ostrowicki, Some effects of multiple injection moulding on selected properties of ABS, Journal of Achievements in Materials and Manufacturing Engineering 37/2 (2009) 361-368.
[42] M. Żenkiewicz, Methods for the calculation of surface free energy of solids, Journal of Achievements in Materials and Manufacturing Engineering 24/1 (2007) 137-145.
[43] L.A. Dobrzański, B. Dołżańska, Structure and properties of sintered tool gradient materials, Journal of Achievements in Materials and Manufacturing Engineering 43/2 (2010) 711-733.
[44] Report of Plastics Europe Foundation, World in 2030 by scientists and futurologists, 2010
[45] http://www.plastech.pl/wiadomosci/artykul_2223_1/Raport-o-tworzywach-swiatowa-produkcja-i-zapotrzebowanie
[46] http://dl.dropbox.com/u/21130258/resources/InformationSheets/Plastics.htm
[47] U.M. Attia, S. Marson, J.R. Alcock, Micro-injection moulding of polymer microfluidic devices, Microfluidics and Nanofluidics 7/1 (2009) 1-28.
[48] http://www.plasticstoday.com/articles/report-highlights-recovery-injection-molding-machine-sales
[49] http://www.plasticseurope.org/pl/document/fakty-o-tworzywach-sztucznych-2010.aspx?FolID=2
[50] http://www.plasticseurope.pl/cust/documentrequest.aspx?DocID=51139
[51] J. Stabik, Ł. Suchoń, M. Rojek, M. Szczepanik, Investigation of processing properties of polyamide filled with hard coal, Journal of Achievements in Materials and Manufacturing Engineering 33/2 (2009) 142-149.
[52] F. La Mantia (Ed.), Handbook of Plastics Recycling, Rapra Technology Ltd, 2002.
[53] L.A. Dobrzański, M. Król, Application of the neural network for Mg-Al-Zn mechanical properties modelling,

Journal of Achievements in Materials and Manufacturing Engineering 37/2 (2009) 549-555.
[54] K.E. Strawhecker, E. Manias, Structure and properties of poly(vinyl alcohol)/ Na+-montmorillonite nanocomposites, Chemistry Materials 12 (2000) 2943-2949.
[55] G. Matula, Carbide alloyed composite manufactured with the PIM method, Archives of Materials Science and Engineering 43/2 (2010) 117-124.
[56] M. Żenkiewicz, J. Richert, Influence of polymer samples preparation procedure on their mechanical properties, Journal of Achievements in Materials and Manufacturing Engineering 26/2 (2008) 155-158.
[57] A.O. Baranov, E.V. Prut, Ultra-high modulus isotactic polypropylene. The influence of orientation drawing and initial morphology on the structure and properties of oriented samples, Journal of Applied Polymer Science 44/9 (2003) 1557-1572.
[58] J.C. Viana, Development of the skin layer in injection moulding: phenomenological model, Polymer 45 (2004) 993-1005.
[59] G. Kalay, M.J. Bevis, The effect of shear controlled orientation in injection moulding on the mechanical properties of an aliphatic polyketone, Journal of Polymer Science: Polymer Physics 35 (1997) 415-430.
[60] J.C. Viana, N. Billon, A.M. Cucha, The thermomechanical environment and the mechanical properties of injection moldings, Polymer Engineering and Science 44/8 (2004) 1522-1533.
[61] M. Szczepanik, J. Stabik, M. Łazarczyk, A. Dybowska, Influence of graphite on electrical properties of polymeric composites, Archives of Materials Science and Engineering 37/1 (2009) 37-44.
[62] J. Stabik, Influence of filler particle geometry on die swell, International Polymer Processing 19/4 (2004) 350-355.
[63] J. Stabik, A. Dybowska, M. Chomiak, Polymer composites filled with powders as polymer graded materials, Journal of Achievements in Materials and Manufacturing Engineering 43/1 (2010) 153-161.
[64] D. Yang, Shape memory alloy and smart hybrid composites — advanced materials for the 21st Century, Materials & Design 21/6 (2000) 503-505.
[65] L.A. Dobrzański, M. Kremzer, M. Drak, Modern composite materials manufactured by pressure infiltration method, Journal of Achievements in Materials and Manufacturing Engineering 30/2 (2008) 121-128.
[66] L.A. Dobrzański, A. Pusz, A.J. Nowak, The elimination of micropores and surface defects in aramid-silicon laminated materials with special properties, Journal of Achievements in Materials and Manufacturing Engineering 35/2 (2009) 121-128.
[67] G. Wróbel, J. Kaczmarczyk, J. Stabik, M. Rojek, Numerical models of polymeric composite to simulate fatigue and ageing processes, Journal of Achievements in Materials and Manufacturing Engineering 34/1 (2009) 31-38.
[68] G. Wróbel, M. Szymiczek, Influence of temperature on friction coefficient of low density polyethylene, Journal of Achievements in Materials and Manufacturing Engineering 28/1 (2008) 31-34.
[69] A. Boczkowska, J. Kapuściński, Z. Lindermann, D. Witemberg-Perzyk, S. Wojciechowski, Composites, Warsaw, 2003 (in Polish).
[70] L.A. Utracki, M.M. Dumoulin, P. Toma, Melt rheology of high density polyethylene/polyamide-6 blends, Polymer Engineering and Science 26/1 (2004) 34-44.
[71] M. Kwaśny, J. Spałek, Supporting the evaluation of tribological processes by measuring and analyzing vibrations generated in the galling test, Tribology 5 (2011) 129-136 (in Polish).
[72] Z. Brytan, M. Bonek, L.A. Dobrzański, W. Pakieła, Surface Layer Properties of Sintered Ferritic Stainless Steel Remelted and Alloyed with FeNi and Ni by HPDL Laser, Advanced Materials Research 291 (2011) 1425-1428.
[73] J. Kaczmarczyk, M. Rojek, G. Wróbel, J. Stabik, A model of heat transfer taking place in thermographic test stand, Journal of Achievements in Materials and Manufacturing Engineering 27/1 (2008) 7-14.
[74] J. Stabik, A. Dybowska, J. Pluszyński, M. Szczepanik, Ł. Suchoń, Magnetic induction of polymer composites filled with ferrite powders, Archives of Materials Science and Engineering 41/1 (2010) 13-20.
[75] W. Kwaśny, K. Gołombek, L.A. Dobrzański, M. Pawlyta, Modelling of a surface with remote geometrical features and their fractal and multifractal characteristics, Materials Engineering 27/5 (2006) 1101-1106 (in Polish).
[76] S. Ghosh, J.C. Viana, R.L. Reis, J.F. Mano, Oriented morphology and enhanced mechanical properties of poly(l-lactic acid) from shear controlled orientation in injection molding, Materials Science and Engineering 490/1-2 (2008) 81-89.
[77] S. Ghosh, J.C. Viana, R.L. Reis, J.F. Mano, Effect of processing conditions on morphology and mechanical properties of injection-molded poly(L-lactic acid), Polymer Engineering and Science 47/7 (2007) 1141-1147.
[78] A.D. Dobrzańska-Danikiewicz, P. Rytlewski, K. Moraczewski, M. Stepczyńska, Development perspectives of selected technologies of polymer surface layers modification, Archives of Materials Science and Engineering 52/1 (2011) 23-45.